MOTION OF NANOSCALE CONTAMINANT PARTICLES IN AIR BEARINGS

By

RICHMOND HARLAN POLWORT

Bachelor of Science

Oklahoma State University

Stillwater, Oklahoma

1996

Submitted to the Faculty of the Graduate College
of the Oklahoma State University
in partial fulfillment of the requirements
for the Degree of
MASTER OF SCIENCE
July, 1999

MOTION OF NANOSCALE CONTAMINANT

PARTICLES IN AIR BEARINGS

Thesis Approved:

Thesis Adviser

Dean of the Graduate College

ACKNOWLEDGMENTS

I would like to thank my advisor, Professor Bjong Yeigh for his patience, determination, tenacity, and prodding to see this research to completion. My home and work schedule made his job far more complicated than it should have but he never gave up, first in me, and second, in the idea that forms the basis of this paper. Without his help, encouragement, and input this thesis would never have been written—at least by me. I began with an advisor and gained a friend. I would also like to thank Charlene Fries, who helped edit and format this work. It was a relief to know my errors were caught by the best.

I would also like to thank the good people of Envirotech Services, Inc., not only for my first position as an engineer, but also for encouraging me to finish this work. Thanks are also due to my colleagues at The Charles Machine Works, Inc., for their encouragement and patience to help me complete this final hurdle.

My family. Where do I start? For every sacrifice I made to return to school, my family made sacrifices ten times over. If nothing else, I hope that my children have learned far earlier than I, that a good education pays a lifetime of returns. I am not so foolish to think that a husband and parent who returns to school in his late thirties can ever hope to succeed without the support of those he loves. Brent and Liesel, your sacrifices helped make this journey possible. Saving the best for last, I would like to thank my beautiful, loving, and patient wife Susan. She has endured, sacrificed, and supported, both financially and spiritually, her student husband. More than just this thesis, this entire journey has been more her accomplishment than mine. Susan, the best is yet to come.

I would also like to express sincere thanks to Seagate Technologies, Oklahoma City Operation, and Dr. Mukund Rao, program manager for their support.

TABLE OF CONTENTS

LIST OF FIGURES

NOMENCLATURE

l	slider length in x-direction
λ_a	molecular mean free path at ambient temperature
h	lubrication film thickness, i.e. height from disk to slider
h_m, h_0	minimum film thickness measured at the trailing edge
H	non-dimensional thickness, $= h / h_0$
Kn	Knudsen number, $= \lambda / h$
Kn_0	characteristic Knudsen number, $= \lambda / h_0$
p	pressure
P_a	ambient pressure
P	non-dimensional pressure, p / p_a
R	universal gas constant
T_∞	characteristic temperature of the gas
T_w	characteristic temperature of the particle wall
x, y, z	spatial coordinates
X, Y, Z	non-dimensional spatial coordinates; x / l, y / l, z / h_0
u, v, w	velocities in x, y, and z directions
U, V, W	non-dimensional velocities in X, Y, and Z directions; $u / \hat{U}, v / \hat{U}, w / \hat{U}$
W	gas bearing load capacity
Λ	bearing number, $= 6\mu\hat{U}l / p_a h_o^2$
ρ_g	gas density
ρ_p	particle density
μ	dynamic viscosity
ν	kinematic viscosity, $= \mu_g / \rho_g$

Q	flow factor correction variable for molecular slip
n	number of current time step
L_1, L_2	linear operator in x and y directions, respectively
N_x, N_y	nodal points in x and y directions, respectively
Δx_i	nodal change in x dimension, $= x_{(i+1)} - x_{(i)}$
θ	slider angle relative to disk
$\hat{U}$	disk speed in X-direction
$\hat{\Omega}$	disk rotational speed, in revolutions per second
C_D	coefficient of drag
C_{Dfm}	coefficient of drag in a free molecular flow
m_p	mass of particle
d	diameter of particle
D	non-dimensional particle diameter, $= d / h_m$
Q_p, Q^*	electrostatic charges on the particle and disk/slider
r	distance between Q_p and Q^*
ε_0	constant, $= 8.854185 \times 10^{-12}\ C^2 / N / m^2$
g_z	gravitational constant, $= 9.81\ m/s^2$
T	non-dimensional time, $= \hat{\Omega} t$

CHAPTER 1

INTRODUCTION

Electronic devices continue to become more commonplace in our everyday lives. If the reader doubts this fact, stop and look around the room. There is probably a television or monitor containing processors presenting graphics that become more realistic with each new model. There could be an electronic clock or wristwatch, a digital music system, a programmable thermostat controlling the room temperature, a digital telephone answering machine, fax machine, cordless telephone, pager, and probably personal computer. Now look out the window. The cars in the street and the planes in the air are more fuel efficient and responsive because of their computer controls. Even the stoplight at the street corner is computer controlled. Our lives are more comfortable, convenient, and productive as a result.

In the early 1970s, pessimistic forecasters predicted massive unemployment as technology and machines replaced workers. The reality was that the opposite occurred. Yes, some jobs were lost forever but entire new industries were created in their place. New millionaires, new factories, new careers, and new job descriptions, unheard of in the 70s, combined to put more people to work than jobs lost. Eliminate every device in our modern world that is computer controlled and our lives would crash to a halt. Society can now no longer separate itself from the computer than it can separate itself from the air we breathe. How have all these electronic machines become so interwoven within the pattern of our lives? The answer: information. Society relies on it. From news shows and near instant stock market reports to satellites that relay communications, take high resolution pictures, and pinpoint locations anywhere on the globe, society and computer provided information are inseparable. Both man and machine base correct decisions on information gathered–and where there is information, then it must be stored and retrieved on demand.

The upcoming millennium has already been titled as the "age of information." The year 2001 brings both promises and problems. One of these new problems is the permanence of our information. The current generation can view original documents that are centuries old. Libraries have discovered procedures and methods of preserving the printed page. However, much of today's information never makes it to the printed page, being distributed though electronic means by email or the Internet. Information storage devices used in the electronic age include magnetic tape, floppy media, CD-ROM, and hard disk drives, all of which have limited lives. Already, magnetic media archives are experiencing severe problems with degradation of microfilm and magnetic tape substrates. Floppy disk media and CD-ROMs both experience degradation problems due to age, physical damage, and contamination. Hard disk drives experience degradation problems also, but today's technology has improved their speed, storage capacity, and has steadily driven down the price until they are the most attractive option for mass storage in today's market. Thus, since hard disk media are today's storage media of choice, much recent effort has involved durability issues.

Disk drive technology development began with the first disk drive, the IBM Model 350, introduced in 1957. This drive also called the Random Access Method of Accounting and Control (RAMAC) was a physically large device. The RAMAC storage media consisted of a stack of 50 disks, each with a diameter of 24 inches and coated with magnetic film. Data were accessed by a pair of air-bearing supported heads mounted on servo-controlled arms, reading or writing to one disk at a time. Storage capacity of this drive, physically larger than twice the combined size of a modern personal computer case and monitor, was 5 MB. The disks rotated at 1200 RPM, a relatively fast speed for a 24-inch disk, yielded a data transfer rate of 12.5kB/s, and rented for $130 a month in 1957 dollars [Berardinis 1995]. Although today this device sounds like a behemoth, in 1957 RAMAC was a major advance in disk drive development.

Previously, data storage utilized tape drives, slow and inexpensive, or magnetic cores, fast and expensive. The magnetic core's expense made the tape drives more attractive, although they consistently suffer from one major drawback--the read/write head must be in close proximity or in contact with the recording tape. At high speeds necessary for fast data transfer, the tape and the head itself have a short useful life. The key development that led to, durable disk drives was the low-mass, air-bearing slider carrying a magnetic head *floating* at a precise distance from the magnetic media surface.

Another factor influencing the development of the disk drive is the disk itself. Disks can be conveniently stacked on one shaft, which simplifies the drive arrangement to move large amounts of magnetic media past a read/write head. The information is stored on the disks in circular tracks with a *bit* as the smallest unit of information. A bit consists of a "0" or a "1". The number of bits written along 1" of one of the circular tracks is called the *linear bit density*. The *track density* is the number of tracks crossed along one inch of the disk's radius. The *areal density* is the product of track density and linear bit density.

Increasing track and areal densities increases drive capacity, given the same size of disk, and also increases data transfer speed since the read/write head encounters more bits over the same distance traveled. Increasing these factors has depended over time on scaling down the following [Ashar 1996]:

1. Reduction of head/disk distance commonly referred to as *flying height.*
2. Reduction of the gap size of the head.
3. Reduction in the thickness of the disk magnetic media.

The following table tracks these factors with a few examples.

TABLE 1.1. DISK DRIVE TECHNOLOGY DEVELOPMENT [ASHAR 1996]

Year	IBM Model	Bit Density Kb/in	Track Density T/in	Areal Density Mb/in^2	Flying Height nm	Gap nm	Thickness nm
1957	350	0.1	20	0.002	20000	25000	30000
1973	3340	5.64	300	1.69	450	1500	1025
1987	3380K	15.2	2088	32.8	216	550	432
1995	Travelstar 2LP	127.2	7257	923	NA	NA	thin film

NA = not available

Note that flying height, head gap, and media thickness decreased in magnitude over the 38-year time span. These changes are directly related to the increase in drive storage capacity and decrease in physical size. Examining changes in disk parameters, note that bit density increased by a factor of approximately 1270, track density increased by a factor of approximately 360, and areal density increased by a factor of approximately 460000.

This large increase in areal density along with manufacturing advances and competition has evolved. In 1957 storage devices were large and heavy enough to use as a boat anchor, rented for $130 per month, and stored 5 MB to a device in 1998 that is the size of a paperback book, has a capacity of 1.6 GB, and can be purchased for $130.

Paralleled by advances in read/write head positioning, flying height has steadily decreased since 1957. Actually, the term "flying height" is a misnomer since the head does not really fly. Instead it rides on the boundary layer of air pulled by friction along the surface of the rotating disk. A close analogy is a water skier. The water skier does not fly along the water but rather rides on top it, held up by the reaction pressure of the water. Sticking with the industry's term, flying height determines, in large part, areal density by directly affecting track density. *Figure 1.1* illustrates the relationship between flying height and zone of influence, which determines the spacing between tracks, that is, the track density.

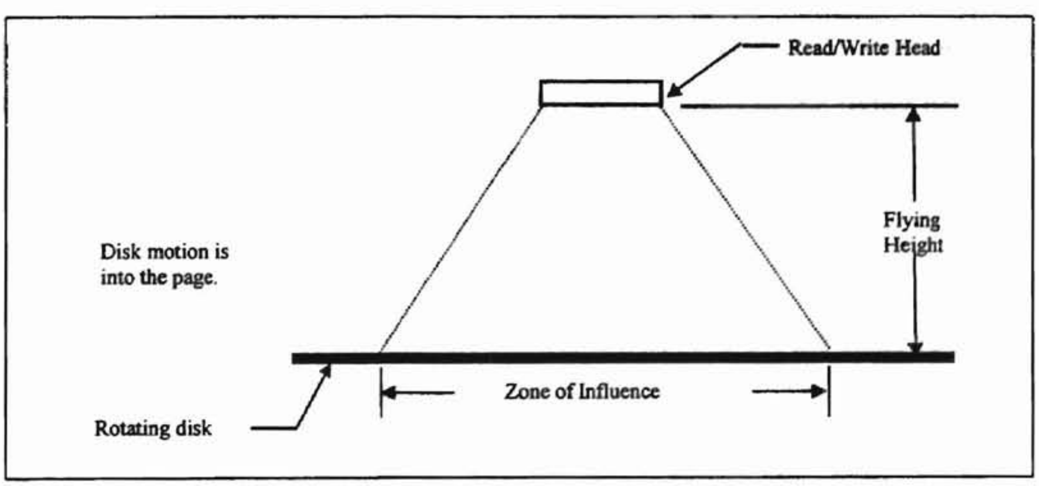

Figure 1.1. Read/Write Head Zone of Influence

Figure 1.1 indicates that for a given flying height, the zone of influence determines the practical track density. If the zone of influence encroaches on a neighboring track, writing to one track will overlap to the next, thus scrambling information on the disk. Compare the zone of influence from *Figures 1.1* and *1.2*. Note the smaller the flying height, the smaller the zone of influence, which will then allow track density to increase.

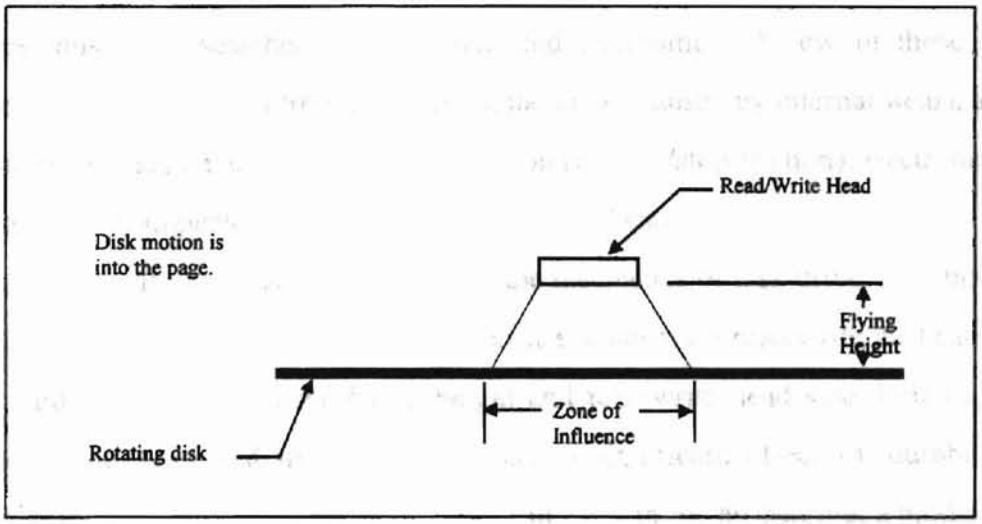

Figure 1.2. Reduced Head Zone of Influence

As the figures illustrate, the smaller the head flying height the smaller the zone of influence and the larger the track density, which ultimately increases disk capacity. However, this reduced flying height demands increased precision and accuracy of the head transport and positioning mechanism. Also, the dynamics of the flying head must be examined closely. Imagine the catastrophic impact of a head contacting a disk spinning at speeds up to 7200 RPM. Not only would data loss occur, but also the head and the disk would be severely damaged.

This brief history of hard disk development is intended to set the stage for the reader to understand a few of the unique issues that confront the hard disk drive industry's future. Hard disk drives are predicted to reach sales in 2010 equal to three times the 1995 figure of 70 million units [Ashar 1996]. Areal densities are expected to increase to 10

GB/in^2, that is 10 billion bits of data on each square inch of recorded surface [Berardinis 1995]. This is equivalent to 625,000 double-spaced typewritten pages, a stack of paper seventeen stories high. This projected figure is 100 times the areal density available in 1995.

With more and more of our information stored by electronic media, durability and preservation of these data are a paramount issue confronting the industry. Many problems must be researched, investigated, and overcome. A few of these include microscopic debris (either introduced at manufacture or caused by internal wear), ambient temperature swings, shock and vibration, stiction (or start/stop friction), electronic noise, recording surface imperfections, and friction-induced heating.

This study will investigate one aspect of the mechanics of disk drive operation--what happens to the path of a debris particle when it encounters a read/write air bearing in a typical hard disk drive. As the flying height and read/write head size decrease, debris buildup on the head and impact damage has a significant effect on durability and performance. To examine the dynamics occurring within the air bearing, a model will be constructed and examined to observe the effect of the air phase flows and pressures upon the trajectory of a debris particle. First, the pressure profile of the air bearing will be calculated; second, these results will be used with Newton's First Law. Forces acting on a particle will be calculated over regular time intervals and the particle will be tracked as it enters the leading edge of the air bearing and proceeds to either impact or escape past the read/write head trailing edge.

CHAPTER 2

AIR BEARING DESIGN AND LUBRICATION

Although not immediately thought of as a lubricant, air has a number of advantages: abundant supply, cleanliness, and lack of environmental and health issues associated with its use compared to a petroleum-based product. However, because of its low viscosity, the speed of an air-lubricated bearing must be several times higher than an oil-lubricated bearing to support the same load. Even though the high speeds required by the air bearing preclude its use in some heavy load applications, there are just as many applications where air bearings are suited or even more ideal than oil-lubricated bearings. They include: machine tool spindles, turbo-machinery, instrument bearings such as gyroscopes, dental drills, textile processing devices, and magnetic media data recording devices such as hard disk drives.

Current disk drive technology has evolved at a pace equaling the evolution of the computer explosion. As it was previously noted in the first chapter, drive densities have increased several thousand times due to advances in read/write head performance, which allowed increases in disk rotational speed and steadily decreasing its flying height. Head materials have moved to lightweight composite alloys, and head support arms and tracking mechanisms have likewise improved. Several models of current drives utilize rotational speeds in excess of 7200 RPM and flying heights in the 30-nanometer range. At these speeds and clearances, characteristics of the pressure generated within the lubrication zone must be known to accurately design components of the head/support arm/positioning mechanisms.

The first read/write head devices were little more than flat pieces of non-conductive material housing a coil of wire. Logical advances in design occurred progressively, beginning with the appearance on the market of a slider with "rails" as shown in *Figure 2.1*. These simple rails have several benefits that greatly improve overall performance of the slider. Benefits include: (1) drag reduction to the slider in flight, (2) diminished contact area in the parking zone resulting in faster takeoff, and (3) debris trapping and flying enhancements in the pressure zones.

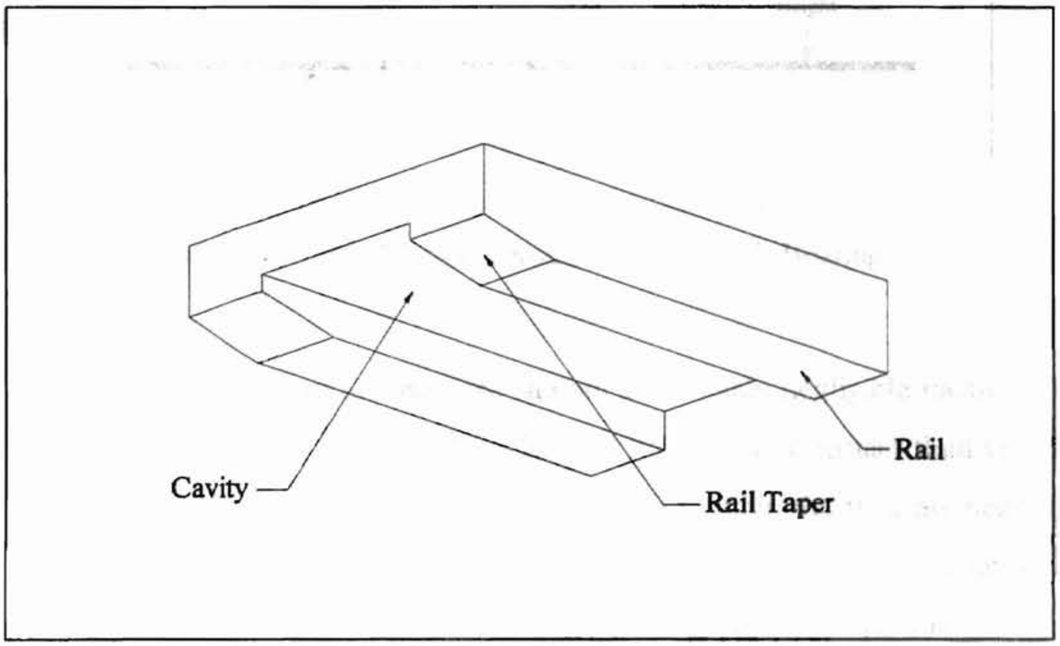

Figure 2.1. Typical View of Simple Slider With Rails

Relying on the pressure generated by the relative motion of sliding surfaces, geometry, and fluid viscosity, hydrodynamic bearings push the contact surfaces apart. Through the converging gap, the fluid enters through the higher of the two opening known as the leading edge and exits the lower trailing edge by the relative motion of the surfaces as shown in *Figure 2.2.* The Reynolds equation calculates the pressure generated between the two surfaces. In the continuum form, the differential equation is obtained from the Navier-Stokes and continuity equations. Derivations can be found in numerous textbooks [Gross et al. 1980, Cameron 1981, Williams 1994].

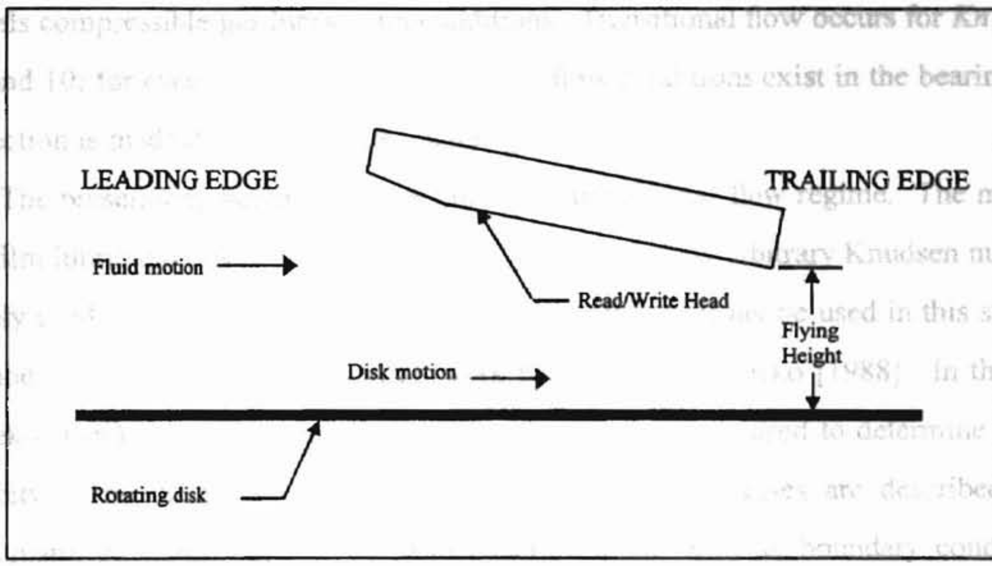

Figure 2.2. Fluid Motion Through a Typical Air Bearing

In the derivation, surfaces are assumed smooth and contain negligible traction. The Newtonian fluid between the surfaces obeys laminar flow rules. Constant fluid viscosity and isothermal conditions also apply. The inertial forces within the fluid are neglected. At the boundaries, nonslip conditions apply [Bhushan 1990]. The above assumptions, Navier-Stokes, and continuity equations yield the following Reynolds equation:

$$\nabla \cdot \left(h^3 P \nabla P\right) = 6\mu V \cdot \nabla P h + 12\mu \frac{\partial P h}{\partial t} \tag{2.1}$$

where h, P, μ, V, and t represent the characteristic length of the flow, bearing pressure, viscosity, velocity, and time, respectively. At steady state operations the time derivative goes to zero and is achieved when the pressure wave having half of the sliding velocity travels across the length of the bearing [White and Nigam 1980].

The extreme values of the clearance (i.e. in the order of 10^{-8}) require a correction to the conventional flow theory, which assumes the flow velocity at the boundary to equal the boundary velocity. This "no-slip" or continuum theory applied to compressible fluid at ultra-low clearances, the continuum Reynolds equation fails to deliver reasonable solutions. The Knudsen number (Kn) is the ratio of molecular mean free path (λ) and the characteristic length of flow (h) [Holman 1972]. For $Kn << 1$, slip flow accurately models compressible gas lubrication conditions. Transitional flow occurs for Kn between 0.1 and 10; for even larger Kn, free molecular flow conditions exist in the bearings. The correction is made through the flow factor, Q.

The present-day bearing designs fall in the transitional flow regime. The molecular gas film lubrication (MGL) equation, which is valid for any arbitrary Knudsen number, is widely used in the hard disk industry. Although MGL will not be used in this study, the method is briefly described based on work by Fukui and Kaneko [1988]. In the Fukui-Kaneko (F-K) model, the classical kinetic theory of gases is used to determine the flow velocity. The distribution of positions and velocities of gases are described by the Boltzmann equation. The Boltzmann equation along with its boundary conditions is linearized to be used in the basic equations for lubrication. The lubrication equation, which is a modified form of the classical Reynolds equation, contains the pressure driven term (or Poiseulle flow) and the shear term (or Couette flow). The pressure inside the bearing is obtained by solving the lubrication equation and balancing the mass flow inside the bearing. In addition, the slip flow Reynolds equation for ultra-thin film lubricating condition can be deduced from MGL [Gans 1985]. In terms of Q, four models including the F-K model are presented.

$$\nabla \cdot \left(Qh^3 P \nabla P\right) = 6\mu V \cdot \nabla Ph + 12\mu \frac{\partial Ph}{\partial t} \tag{2.2}$$

TABLE 2.1. FOUR MODELS AND THEIR CORRESPONDING FLOW FACTORS

$Q = 1$	Continuum
$Q = 1 + 6a\frac{Kn_0}{PH}$	First-Order Slip
$Q = 1 + 6\frac{Kn_0}{PH} + 6\left(\frac{Kn_0}{PH}\right)^2$	Second-Order Slip
$Q = f\left(\frac{Kn_0}{PH}\right)$	Fukui-Kaneko

Note: $a = \frac{2-\alpha}{\alpha}$ α = accommodation factor

Couette flow becomes significant with increasing *Kn*. The continuum model overestimates load capacity W. Burgdorfer's first-order slip model [1959] slightly overestimates W, and the second-order slip model [Hsia and Domoto 1983] underestimates W by a small amount. The F-K model [Fukui and Kaneko 1988] falls between the two slip models. For this study, the first-order slip model will be used as it provides a reasonable estimation for the bearing geometry used.

CHAPTER 3

NUMERICAL SOLUTION FOR GAS BEARINGS AT HIGH BEARING NUMBERS

The bearing number, Λ, is a nondimensional quantity measuring the ratio between two types of flows present in the air bearing. Poiseulle flow is driven by pressure gradients present at the interface. Couette flow, on the other had, is shear driven by flow velocities at the boundaries. The bearing number then is the ratio of Couette flow to Poiseulle flow. Dividing the first term in the Reynolds equation by $p_a h_0^2/l$ yields Λ. Present-day disk drives have the minimum clearance, h_0, in the order 10^{-8} m. With h_0^2 in the denominator and the boundary velocity on the order of 10, the corresponding bearing number can exceed 20,000. At these extremes, solutions of the Reynolds equation become numerically unstable.

Although the finite element method (FEM) has been used in the solution of the Reynolds equation [Tokuyama and Hirose 1994], the finite difference method appears to be the method of choice for many researchers [Castelli and Pirvics 1968, Coleman 1968, Fukui and Kaneko 1988, Hu and Bogy 1997]. Singular perturbation techniques for asymptotic solution [DiPrima 1968] had also been tried but had not gained popular support. Recent solutions have also utilized advanced techniques such as the control volume method [Hu and Bogy 1998]. In addition to the above numerical techniques, a widely known differencing technique—an alternating direction implicit (ADI) method—is chosen to solve the Reynolds equation with first-order slip in this study.

A factored implicit scheme (FIS) is presented in this chapter which closely follows White and Nigam's 1980 paper. FIS is an alternating direction implicit (ADI) method that splits the multidimensional time-dependent problem into a series of linear operators in their respective directions. The resulting matrix is tridiagonal, which leads to simple Gaussian elimination in the solution. For this reason, the ADI method has been very successful with the Dirichlet problem for Laplace and Poisson equations [Kreyszig 1993]. Splitting operators in two space dimensions is often referred to as the Peaceman-Rachford ADI method [Akai 1994].

The solution for pressure under the flat slider, obtained through FIS for the first order slip theory outlined by White and Nigam [1980], is presented below with corrections. The general dimensional form of the lubrication equation with first-order slip can be written in the following vector form:

$$\nabla\cdot\left(h\ P\nabla P\right)+6\lambda_a P_a \nabla\cdot\left(h^2\nabla P\right)=6\mu V\cdot\nabla Ph+12\mu\frac{\partial Ph}{\partial t} \tag{3.1}$$

where h, P, λ_a, P_a, μ, and t represent the gas bearing spacing, gas bearing pressure, mean free path of the gas at ambient pressure, ambient pressure, lubricant viscosity, and time, respectively. The two dependent variables (i.e. P and h) in *Equation 3.1* can be combined to yield *Equation 3.2*, where Z represents the product of bearing pressure and clearance:

$$\nabla\cdot\left(hZ\nabla Z-Z^2\nabla h+6\lambda_a P_a\left(h\nabla Z-Z\nabla h\right)\right)=6\mu V\cdot\nabla Z+12\mu\frac{\partial Z}{\partial t} \tag{3.2}$$

Gradient and divergence in the above lubrication equation are then completed and the resulting terms are grouped in the x- and y-directions. The subscripts represent partial derivatives in their respective directions x and y and in time t:

$$\begin{aligned}&\nabla\cdot(hZZ_x-Z^2h_x+6\lambda_a P_a\left(hZ_x-Zh_x\right)-6\mu V_x Z\\&+hZZ_y-Z^2h_y+6\lambda_a P_a\left(hZ_y-Zh_y\right)-6\mu V_{yx}Z)\quad=12\mu Z_t\end{aligned} \tag{3.3}$$

The right-hand side of the above equation contains a time-dependent derivative Z_t. Both Z and Z_t are expanded about n time levels using the trapezoidal formula, where the superscripts *(n)* and *(n+1)* represent time steps. The left-hand side is also expanded in time, yielding *Equation 3.4*:

$$Z^{(n+1)}=Z^{(n)}+\frac{\Delta t}{2}\left(Z_t^{(n)}+Z_t^{(n+1)}\right)+O\left(\Delta t^3\right) \tag{3.4}$$

The resulting nonlinear equation is then ordered by casting Z and its derivatives in the spatial domain on the left, and h and its derivatives on the right along with Z and its derivatives in the time domain as shown in *Equation 3.5*:

$$
\begin{aligned}
&\left(Z^{(n+1)} - Z^{(n)}\right) - \frac{\Delta t}{24\mu}\{((hZ_x - 2Zh_x - 6\lambda_a P_a h_x - 6\mu V_x)^{(n)}(Z^{(n+1)} - Z^{(n)}))_x \\
&\qquad + ((hZ + 6\lambda_a P_a h)^{(n)}(Z^{(n+1)} - Z^{(n)})_x)_x \\
&\qquad + ((hZ_y - 2Zh_y - 6\lambda_a P_a h_y - 6\mu V_y)^{(n)}(Z^{(n+1)} - Z^{(n)}))_y \\
&\qquad + ((hZ + 6\lambda_a P_a h)^{(n)}(Z^{(n+1)} - Z^{(n)})_y)_y\} \\
&= \frac{\Delta t}{24\mu}\{((hZ_x + 6\lambda_a P_a Z_x)^{(n)}(h^{(n+1)} - h^{(n)}))_x \\
&\qquad + ((-Z^2 - 6\lambda_a P_a Z)^{(n)}(h_x^{(n+1)} - h_x^{(n)}))_x \\
&\qquad + ((hZ_y + 6\lambda_a P_a Z_y)^{(n)}(h^{(n+1)} - h^{(n)}))_y \\
&\qquad + ((-Z^2 - 6\lambda_a P_a Z)^{(n)}(h_y^{(n+1)} - h_y^{(n)}))_y\}
\end{aligned}
\tag{3.5}
$$

Finite difference derivatives in x and y are introduced to the equation in the form of δ_x and δ_y. The difference operators are then split into the linear operators L_1 and L_2, where the former difference operator is applied in the x-direction and the latter in y:

$$
\begin{aligned}
L_1(x) &= \frac{\Delta t}{24\mu}\{\delta_x(hZ_x - 2Zh_x - 6\lambda_a P_a h_x - 6\mu V_x)^{(n)} \\
&\qquad + \delta_x(hZ + 6\lambda_a P_a h)^{(n)}\delta_x\}
\end{aligned}
\tag{3.6}
$$

$$
\begin{aligned}
L_2(y) &= \frac{\Delta t}{24\mu}\{\delta_y(hZ_y - 2Zh_y - 6\lambda_a P_a h_y - 6\mu V_y)^{(n)} \\
&\qquad + \delta_y(hZ + 6\lambda_a P_a h)^{(n)}\delta_y\}
\end{aligned}
\tag{3.7}
$$

$$
[1 - L_1 - L_2]\left(Z^{(n+1)} - Z^{(n)}\right) = \phi + O(\Delta t^3) \tag{3.8}
$$

where ϕ is the right-hand side from *Equation 3.5*. Consequently, the nonlinear lubrication problem is cast into two sets of linear lubrication equations. The linear operators are further factored. The truncation error in the resulting *Equation 3.9* is of order Δt^3:

$$
[1 - L_1][1 - L_2]\left(Z^{(n+1)} - Z^{(n)}\right) - L_1 L_2\left(Z^{(n+1)} - Z^{(n)}\right) = \phi + O\left(\Delta t^3\right) \tag{3.9}
$$

The term containing the product of two linear operators L_1 and L_2 is multiplied and divided by Δt. This term is also of order Δt^3 and omitted for second-order accuracy solution in time. In the numerical procedure, the factored linear operators are applied separately and the results combined. In other words, the L_1 operator is carried out first, and its solutions are used in the L_2 operation as shown in *Equations 3.10a* and *3.10b*. The solution vectors ΔZ^* and ΔZ^n represent the difference ($Z^{(n+1)}$ -$Z^{(n)}$) in the *x*- and *y*-directions, respectively:

$$[1 - L_1](\Delta Z^*) = \phi \tag{3.10a}$$

$$[1 - L_{21}](\Delta Z^{(n)}) = \Delta Z^* \tag{3.10b}$$

Indeed, the two-dimensional nonlinear lubrication problem has been reduced to two one-dimensional linear operators. If there are N_x and N_y nodal points in *x* and *y*, respectively, the factored implicit scheme presented above will require solutions of N_x by N_x tridiagonal matrices. There would be N_y of these matrices in the *x*-direction. In the *y*-direction, N_x number of N_y by N_y matrices will require tridiagonal inversion.

In the case of hard disk drives, reduction in bearing clearance has significantly increased Λ. As noted in the first chapter, reducing the clearance has significantly increased track densities in the disk media. Although the benefits of ever-greater track densities outweigh costs associated with it, further lowering of bearing clearances pose numerical difficulties in air bearing design. First, continuum solutions are no longer valid in such regions. This question has been addressed by the development of MGL [Fukui and Kaneko 1988]. Second, in traditional finite difference schemes with uniform meshes nonphysical (i.e. numerical) oscillations propagate throughout the fluid, rendering the numerical solution useless. The question is addressed in this study through variable meshing [White and Nigam 1980].

What goes into the air bearing must come out. As the mass flux is balanced, the pressure gradient is extremely steep at the trailing edge. Near the leading edge, the pressure gradient is very gradual. To account for such change, variable grids are used—coarser meshes between the nodes near the leading edge and finer meshes between the nodes near the trailing edge. Using fine meshes everywhere can also solve this issue, although such a method would not be prudent due to computational intensity. A possible way to introduce variable meshes is by sizing each subsequent node by a geometric proportion of the previous node:

$$\Delta x(i+1) = \Delta x(i) * GridFactor \tag{3.11}$$

Although arithmetic progression would work in theory, it appears that a grid factor based on minimum spacing required to build the boundary layer seems most prudent.

The finite difference derivatives for Z with variable meshes include:

$$Z_{xx}(i,j) = \sum_{k=1}^{3} A_k(i) Z(i+2-k, j) \tag{3.12a}$$

$$Z_{x}(i,j) = \sum_{k=1}^{3} C_k(i) Z(i+2-k, j) \tag{3.12b}$$

$$Z_{yy}(i,j) = \sum_{k=1}^{3} B_k(i) Z(i, j+2-k) \tag{3.12c}$$

$$Z_{y}(i,j) = \sum_{k=1}^{3} D_k(i) Z(i, j+2-k) \tag{3.12d}$$

where the coefficients $A_k(\,)$, $B_k(\,)$, $C_k(\,)$, and $D_k(\,)$ represent grid differences in x and y based on a three-point difference scheme:

$$A_1(i) = \frac{2}{\Delta x(i)\left[\Delta x(i-1)\Delta x(i)\right]} \tag{3.13a}$$

$$A_2(i) = \frac{-2}{\Delta x(i-1)\Delta x(i)} \tag{3.13b}$$

$$A_3(i) = \frac{2}{\Delta x(i-1)\left[\Delta x(i-1)+\Delta x(i)\right]} \tag{3.13c}$$

$$B_1(i) = \frac{2}{\Delta y(i)\left[\Delta y(i-1)\Delta y(i)\right]} \tag{3.14a}$$

$$B_2(i) = \frac{-2}{\Delta y(i-1)\Delta y(i)} \tag{3.14b}$$

$$B_3(i) = \frac{2}{\Delta y(i-1)\left[\Delta y(i-1)+\Delta y(i)\right]} \tag{3.14c}$$

$$C_1(i) = \frac{\Delta x(i-1)}{\Delta x(i)\left[\Delta x(i-1)\Delta x(i)\right]} \tag{3.15a}$$

$$C_2(i) = \frac{\Delta x(i)-\Delta x(i-1)}{\Delta x(i-1)\Delta x(i)} \tag{3.15b}$$

$$C_3(i) = \frac{-\Delta x(i)}{\Delta x(i-1)\left[\Delta x(i-1)+\Delta x(i)\right]} \tag{3.15c}$$

$$D_1(i) = \frac{\Delta y(i-1)}{\Delta y(i)\left[\Delta y(i-1)\Delta y(i)\right]} \tag{3.16a}$$

$$D_2(i) = \frac{\Delta y(i)-\Delta y(i-1)}{\Delta y(i-1)\Delta y(i)} \tag{3.16b}$$

$$D_3(i) = \frac{-\Delta y(i)}{\Delta y(i-1)\left[\Delta y(i-1)+\Delta y(i)\right]} \tag{3.16c}$$

The spatial increment in x and y use a forward difference scheme (i.e. $\Delta x(i) = x(i+1) - x(i)$ and $\Delta y(i) = y(i+1) - y(i)$).

The variable grid scheme in conjunction with the ADI method yields the following linear operators L_1 and L_2 and the right-hand side term ϕ.

$$
\begin{aligned}
L_1(\Delta Z^*)_{(i,j)} &= \frac{\Delta t}{24\mu}\{[(2hZ_x - Zh_x - 6\mu V_x)C_3(i) \\
&+ (Z + 6\lambda_a P_a)hA_3(i)]^{(n)}(\Delta Z^*)_{(i-1,j)} + [hZ_{xx} - h_x Z_x \\
&- (2Z + 6\lambda_a P_a)h_{xx} + (2hZ_x - Zh_x - 6\mu V_x)C_2(i) \\
&+ (Z + 6\lambda_a P_a)hA_2(i)]^{(n)}(\Delta Z^*)_{(i,j)} + [(2hZ_x - Zh_x \\
&- 6\mu V_x)C_1(i) + (Z + 6\lambda_a P_a)hA_1(i)]^{(n)}(\Delta Z^*)_{(i+1,j)}\}
\end{aligned}
\tag{3.17}
$$

$$
\begin{aligned}
L_2(\Delta Z'')_{(i,j)} &= \frac{\Delta t}{24\mu}\{[(2hZ_y - Zh_y - 6\mu V_y)D_3(j) \\
&+ (Z + 6\lambda_a P_a)hB_3(j)]^{(n)}(\Delta Z'')_{(i,j-1)} + [hZ_{yy} - h_y Z_y \\
&- (2Z + 6\lambda_a P_a)h_{yy} + (2hZ_y - Zh_y - 6\mu V_y)D_2(j) \\
&+ (Z + 6\lambda_a P_a)hB_2(j)]^{(n)}(\Delta Z'')_{(i,j)} + [(2hZ_y - Zh_y \\
&- 6\mu V_y)D_1(j) + (Z + 6\lambda_a P_a)hB_1(j)]^{(n)}(\Delta Z'')_{(i,j+1)}\}
\end{aligned}
\tag{3.18}
$$

$$
\begin{aligned}
\phi &= 2\frac{\Delta t}{24\mu}\{[(Z + 6\lambda_a P_a)(Z_{xx} + Z_{yy}) + (Z_x Z_x + Z_y Z_y)]h \\
&- ZZ_x h_x - 6\mu V_x Z_x\}
\end{aligned}
\tag{3.19}
$$

A *Mathcad* solution is appended. Particle motion in the recessed region of the slider is modeled in Chapter 4. The recessed region is in the centerline of the air bearing. The pressure in this region is equivalent to the infinitely wide bearing with no rails or series of one-dimensional solutions of the same kind. *Table 3.1* lists the bearing and lubrication parameters, and the corresponding pressure profile is depicted in *Figure 3.1*. The theoretical maximum for the normalized pressure (P/P_a) is 3.0. If the bearing were much narrower, side flow would reduce this maximum considerably.

TABLE 3.1. BEARING LUBRICATION PARAMETERS

Fluid Properties			
μ	$= 18*10^{-6}$	Pa*s	dynamic viscosity of air at 71oF
λ	$= 6.35*10^{-8}$	m	mean free path of air
p_o	$= 1.01*10^{5}$	Pa	ambient atmospheric pressure
Bearing Geometry			
h_m	$= 127*10^{-9}$	m	minimum height of slider above disk
α	$= 100$	μ rad	slider angle relative to disk
V_x	$= 50.8$	$m*s^{-1}$	disk speed in x-direction
V_y	$= 0$	$m*s^{-1}$	disk speed in y-direction
L_x	$= 2.54*10^{-3}$	m	slider length in x-direction
Numerical Grid			
Δx_{min}	$= 1.27*10^{-6}$	m	smallest change in x-direction spacing
$\dfrac{\Delta x_{(i)}}{\Delta x_{(i+1)}}$	$= 1.112 =$ GM		grid factor (or multiplier)
Δt	$= 5*10^{-5}$	s	integral time step

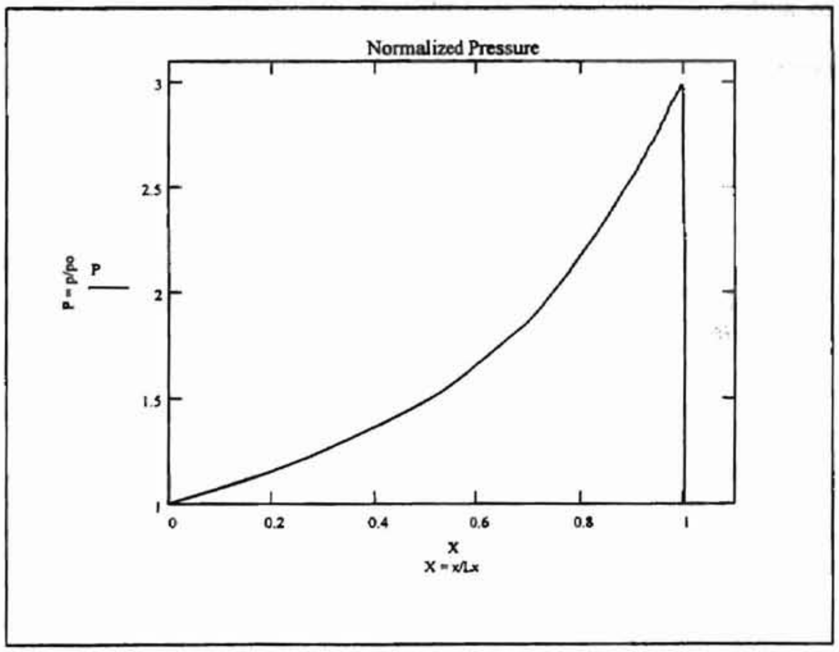

Figure 3.1. Centerline Pressure Profile

CHAPTER 4

CONTAMINANT PARTICLE MOTION AT HIGH BEARING NUMBERS

Loose particle(s) inside hard disk drives can be detrimental. With air bearing clearance in the submicron level, the particle size does not have to be large to cause serious damages to the disk. Whether the loose particles come from fine particles accumulated on the leading edge tapers [Koka and Kumaran 1991] or from contaminant whiskers that broke off from the trailing edge [Hiller and Singh 1991], these particles can lead to third-body abrasions of disk surface. Several questions arise. First, inside the air bearing, where do trapped particles go? Do they adhere to the slider/disk or wash out of the bearing? Second, what operating conditions force loose particles to move towards the slider? When do they move toward the disk surface? Perhaps some of the answers lie in the particle motion study.

Zhang and Bogy [1997] considered the effects of lift on the motion of particles in the recessed region of a slider. This study examined four important forces inside the air bearing—drag force, Saffman lift force, Magnus lift force, and gravity force. The numerical investigation revealed a relationship between the lift forces and physical parameters such as particle size, relative velocity, and particle density. Magnus force results showed little effect and will not be considered in this study. However, one force not considered in Zhang and Bogy's study is the electromagnetic force, which is the focus of this study. Before the effect(s) of electromagnetic force on the particle motion can be considered, a detailed analysis of governing equations and their solutions leading to particle motion is presented.

Consider an air bearing assembly shown below in *Figure 4.1*. A slider of length, l, and pitch, θ, rides above a disk spinning at $\hat{\Omega}$ (or slides with a linear velocity $\hat{U}$). The slider and disk are separated by h, which is minimum (h_m) at the trailing edge. In the present study, the minimum clearance, slider length, and pitch angle are taken in the neighborhood of 3 μm, 2 mm, and 150 μrad, respectively.

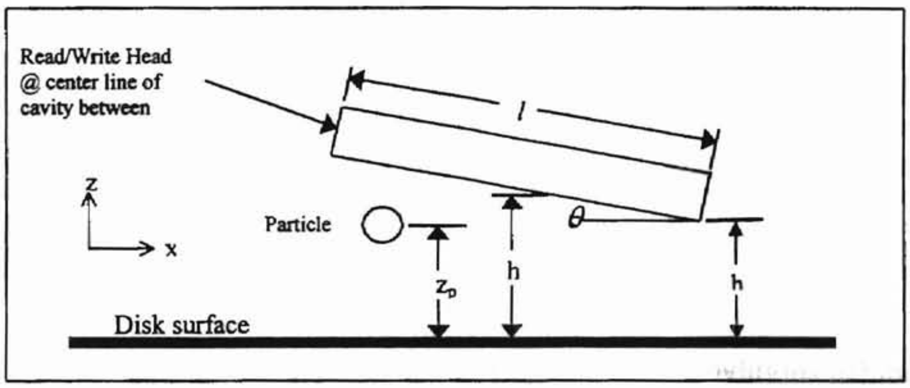

Figure 4.1. Simplified Slider-Disk Assembly

A spherical particle of diameter, d, enters the air bearing. In the present study, d is restricted to the range of 100 to 350 nm. The motion of a particle inside an air bearing can be described fully by its position vector $\vec{x}_p$ (x_p, y_p, z_p) and velocity vector $\vec{v}_p$ (u_p, v_p, w_p) in the Cartesian coordinate system. Purely from the Newtonian mechanics viewpoint, the First Law provides the relationship between external forces and their effects on the particle motion:

$$\vec{F}_p = m_p \frac{d\vec{v}_p}{dt} \tag{4.1}$$

$$\vec{v}_p = \frac{d\vec{x}_p}{dt} \tag{4.2}$$

where $\vec{F}_p$, $\vec{v}_p$, $\vec{x}_p$, and m_p represent force, velocity, position, and mass of the particle, respectively. Derivatives are taken with respect to time, and the arrows indicate vector quantities. *Equations 4.1* and *4.2* require solving six coupled differential equations simultaneously at each time step.

Liu and his colleagues [1965] used the Boltzmann equation to study the kinetic theory of sphere drag in transition flows and found that the ratio of the drag coefficient, C_D, normalized by its corresponding drag coefficient for almost-free molecular flow, C_{Dfm}, was independent of the speed ratio, s:

$$\frac{C_D}{C_{Dfm}} = 1 - \frac{B(s)}{Kn} \tag{4.3}$$

where $B(s)$ is essentially 0.15 and Kn is the Knudsen number. The speed ratio of a particle in air almost-free of molecules is calculated from *Equation 4.4*:

$$s = \frac{\left|\vec{v}_g - \vec{v}_p\right|}{\left(2RT_\infty\right)^{1/2}} \tag{4.4}$$

For a spherical particle entering the air bearing, the flow conditions exhibit almost-free molecular flow regime ($0.5 < Kn < 10$) given by Liu. The drag coefficient for almost-free molecular flow is written as [Zhang and Bogy 1997]:

$$C_{Dfm} = \frac{2}{s^3}\left[\frac{4s^4 + 4s^2 - 1}{4s} erf(s) + \frac{e^{-\frac{s^2}{2}}}{\sqrt{\pi}}\left(s^2 + \frac{1}{2}\right)\right] + \frac{2\sqrt{\pi}}{3s}\sqrt{\frac{T_w}{T_\infty}} \tag{4.5}$$

Substituting *Equation 4.5* into *Equation 4.3*, the drag coefficient can be obtained. Then the resulting drag force, f_D, on the particle can be written in terms of C_D:

$$f_D = \frac{\pi}{8} C_D \rho_g d^2 \left|\vec{v}_g - \vec{v}_p\right| \left(\vec{v}_g - \vec{v}_p\right) \tag{4.6}$$

where ρ_g is the density of air. Unless otherwise noted, p and g denote particle and air, respectively.

In addition to particle drag, the particle can be "lifted" in the direction perpendicular to the fluid flow. This force is known as the Saffman lift force. If particle velocity is greater than fluid velocity, the force will point upward toward the slider, and vice versa

[Saffman 1965]. This result is valid for very small Reynolds numbers. The lift force in the z-direction then has the magnitude,

$$f_S = K(\Delta V)\mu a^2 \sqrt{\frac{\kappa}{\nu}} + O\left(\sqrt{\frac{1}{\nu}}\right) \tag{4.7}$$

where ΔV, κ, and ν represent relative velocity of the sphere (with respect to fluid), magnitude of the velocity gradient, and kinematic viscosity. The constant, K, is the numerical integral of the three-dimensional Fourier transform of the velocity field and its numerical value reported by Saffman and recalculated by Zhang and Bogy is 6.46. The relative velocity ΔV is given by the equation,

$$\Delta V = \frac{(u_p - u_g)u_g + (v_p - v_g)v_g}{\sqrt{u_g^2 + v_g^2}} \tag{4.8}$$

and the velocity gradient is defined by

$$\kappa = \left| \frac{u_g}{\sqrt{u_g^2 + v_g^2}} \frac{\partial u_g}{\partial z} + \frac{v_g}{\sqrt{u_g^2 + v_g^2}} \frac{\partial v_g}{\partial z} \right| \tag{4.9}$$

As the sphere flows through air, the gravitational pull (or push) is of order d^3. Compared to the drag components in the x-y plane, which is of order d^2, only the z-component is significant. The force due to gravity is written as

$$f_G = \frac{1}{6}\pi d^3 (\rho_g - \rho_p) g_z \tag{4.10}$$

where g_z is the gravitational constant.

It is difficult to measure exactly how much electrostatic charge is present in a contaminant particle. Consequently, the Bohr radius is used to estimate the maximum charge on an aluminum sphere. Given the diametrical range of 100 to 350 nm, a 100-nm aluminum sphere may hold roughly 844 million hydrogen atoms or equivalents. A 350-nm sphere can hold in excess of 36 billion hydrogen atoms or equivalents. Assuming that each hydrogen atom is ionized, 100 and 350 nm aluminum sphere can be charged on the order of 1.3516 x 10^{-10} Coulombs and 5.7950 x 10^{-9} Coulombs, respectively. Coulomb's Law gives the electrostatic force:

$$f_E = \frac{1}{4\pi\varepsilon_0}\frac{Q_p Q^*}{r^2} = 8.9918\times 10^6 \frac{Q_p Q^*}{r^2} \tag{4.11}$$

where Q_p and Q^* measure electrostatic charges on the particle and slider (or disk). The distance between Q_p and Q^* is the value, r. The electrostatic force above is expressed in Newtons.

Drag, Saffman, gravity, and electrostatic forces combine to influence particle motion. The left-hand side of *Equation 4.1* can now be written as the sum of the individual forces expressed above.

$$\bar{F}_p = f_D + f_S + f_G + f_E \tag{4.12}$$

Saffman, gravity, and electrostatic forces all act in the direction perpendicular to the fluid flow. Drag affects all three orthogonal directions.

Dimensional coordinates and bearing parameters are made dimensionless. Unless otherwise noted, lowercase variables are cast into dimensionless uppercase variables. Horizontal components are normalized with respect to slider length, and vertical components are divided by minimum height. The product of rotational speed $\hat{\Omega}$ and circumference yields the linear sliding velocity $\hat{U}$. Velocity components are normalized by $\hat{U}$, and dimensional time is multiplied by $\hat{\Omega}$ to produce T:

$$X = \frac{x}{l} \quad Y = \frac{y}{l} \quad Z = \frac{z}{h_m} \tag{4.11}$$

$$U = \frac{u}{\hat{U}} \quad V = \frac{v}{\hat{U}} \quad W = \frac{w}{\hat{U}} \tag{4.12}$$

$$T = \hat{\Omega} t \tag{4.13}$$

Applying the chain rule conveniently transforms other dimensional variables into dimensionless variables. For example,

$$\frac{dX_p}{dT}=\frac{dx_p}{dt}\frac{dt}{dT}\frac{dX_p}{dx_p}=\frac{\hat{U}}{\hat{\Omega}l}U_p \tag{4.14a}$$

$$\frac{dY_p}{dT}=\frac{\hat{U}}{\hat{\Omega}l}V_p \tag{4.14b}$$

$$\frac{dZ_p}{dT}=\frac{\hat{U}}{\hat{\Omega}h_m}W_p \tag{4.14c}$$

Acceleration components in the three orthogonal coordinates are also given by the chain rule. *Equations 4.1* and *4.6* are combined. Dividing the force components by m_p, acceleration components in X and Y are:

$$\frac{dU_p}{dT}=\frac{3}{4}\frac{\hat{U}}{\hat{\Omega}h_m}\frac{\rho_g}{\rho_p}\frac{C_D}{D}\overline{U}\left(U_g-U_p\right) \tag{4.15a}$$

$$\frac{dV_p}{dT}=\frac{3}{4}\frac{\hat{U}}{\hat{\Omega}h_m}\frac{\rho_g}{\rho_p}\frac{C_D}{D}\overline{U}\left(V_g-V_p\right) \tag{4.15b}$$

where $\overline{U}$ is the quotient of the velocity norm and the sliding velocity.

$$\left|\overline{v}_g-\overline{v}_p\right|=\hat{U}\overline{U} \tag{4.16}$$

The dimensionless diameter, D, is obtained from dividing the particle diameter by the minimum height. The Z-component acceleration has contributions from drag, Saffman, gravity, and electrostatic forces:

$$\begin{aligned}\frac{dW_p}{dT}=&\frac{3}{4}\frac{\hat{U}}{\hat{\Omega}h_m}\frac{\rho_g}{\rho_p}\frac{C_D}{D}\overline{U}\left(W_g-W_p\right)\\&+\frac{9.69}{\pi}\frac{\hat{U}\widetilde{U}}{\hat{\Omega}h_m D}\frac{\rho_g}{\rho_p}\sqrt{\frac{v_g h_m \kappa}{\hat{U}^2 h_m}}\\&+\frac{\hat{U}}{\hat{\Omega}h_m}\left(\frac{\rho_g}{\rho_p}-1\right)\frac{h_m}{\hat{U}^2}g\\&+\frac{1.717308\times10^{10}}{\rho_p r^2 h_m^3 D^3}\frac{Q_p Q^*}{\hat{\Omega}\hat{U}}\end{aligned} \tag{4.17}$$

where $\widetilde{U}=\dfrac{\Delta U}{\hat{U}}$.

As previously stated, *Equations 4.1* and *4.2* comprise a system of six coupled differential equations at each time step, ΔT. These equations are solved using the classical Runge-Kutta numerical method. The R-K method is of significant practical importance and can be shown to have a truncation error per step on the order of ΔT^5 [Kreyszig 1993]; therefore the method is a fourth-order method. A brief explanation, as R-K relates to this problem, is given here. The *Mathcad* file is appended.

On examination, the R-K method is an ordered method where the value at the next time step is accurately calculated using values from the current time step and is initiated using values from the initial conditions which are known. Note no assumptions or estimates of future values are used. Each new value is calculated from known values at the respective step. *Equations 4.1* and *4.2* can be generalized in the component form as:

$$\frac{d\gamma_i}{dT} = fn(T,\gamma_1,\gamma_2,\gamma_3,\gamma_4,\gamma_5,\gamma_6) \qquad i = 1,2,\ldots,6 \qquad (4.18a)$$

with the initial conditions:

$$\gamma_i(T_o) = \gamma_{io} \qquad i = 1,2,\ldots,6 \qquad (4.18b)$$

where γ_i ($i = 1, 2, \ldots, 6$) represent, respectively X_p, Y_p, Z_p, U_p, V_p, W_p, the components of the position vectors $\bar{X}p$, $\bar{Y}p$, $\bar{Z}p$; the functions fn_i represent the RHS of *Equations 4.14, 4.15,* and *4.17*. For instance, fn_4 equals the RHS of *Equation 4.15a*, fn_5 equals the RHS of *Equation 4.15b*, and fn_6 equals the RHS of *Equation 4.17*. Written as *Equation 4.18* the last three coupled equations at $i = 4, 5, 6$ are solved first at each time step using the R-K method, written as:

$$\gamma_{i,n+1} = \gamma_{i,n} + \frac{\Delta T}{6}(k_{1,i} + 2k_{2,i} + 2k_{3,i} + k_{4,i}) \qquad i = 4, 5, 6 \qquad (4.19a)$$

$$k_{1,i} = fn_i(T_n, \gamma_{4,n},\ldots,\gamma_{6,n}) \qquad (4.19b)$$

$$k_{2,i} = fn_i(T_n + \frac{\Delta T}{2}, \gamma_{4,n} + \frac{\Delta T}{2}k_{1,4},\ldots,\gamma_{6,n} + \frac{\Delta T}{2}k_{1,6}) \qquad (4.19c)$$

$$k_{3,i} = fn_i(T_n + \frac{\Delta T}{2}, \gamma_{4,n} + \frac{\Delta T}{2}k_{2,4},\ldots,\gamma_{6,n} + \frac{\Delta T}{2}k_{2,6}) \qquad (4.19d)$$

$$k_{4,i} = fn_i(T_n + \Delta T, \gamma_{4,n} + \Delta T k_{3,4},\ldots,\gamma_{6,n} + \Delta T k_{3,6}) \qquad (4.19e)$$

where ΔT is the integral time step and n represents the nth iteration. Once solutions at time step $n+1$ are found, the time derivatives in *Equations 4.14a, 4.14b,* and *4.14c* are rewritten as simple slopes:

$$\frac{dX_p}{dT} \cong \frac{X_{p(n+1)} - X_{p(n)}}{\Delta T} \tag{4.20a}$$

$$\frac{dY_p}{dT} \cong \frac{Y_{p(n+1)} - Y_{p(n)}}{\Delta T} \tag{4.20b}$$

$$\frac{dZ_p}{dT} \cong \frac{Z_{p(n+1)} - Z_{p(n)}}{\Delta T} \tag{4.20c}$$

The slope equations above accurately approach the true value of the derivatives using a very small time step, ΔT. *Equation 4.20* is substituted into *Equation 4.14* and solved for the parameter at time step $(n + 1)$. Thus, *Equation 4.14* is recast as:

$$X_{p(n+1)} = X_{p(n)} + \Delta T\left(\frac{\hat{U}}{\hat{\Omega} l} U_{p(n+1)}\right) \tag{4.21a}$$

$$Y_{p(n+1)} = Y_{p(n)} + \Delta T\left(\frac{\hat{U}}{\hat{\Omega} l} V_{p(n+1)}\right) \tag{4.21b}$$

$$Z_{p(n+1)} = Z_{p(n)} + \Delta T\left(\frac{\hat{U}}{\hat{\Omega} h_m} W_{p(n+1)}\right) \tag{4.21c}$$

With the results from *Equation 4.19,* all variables on the RHS contained in *Equation 4.21* are known. Once solved, all parameters in the acceleration equations are updated and the procedure repeats. The iterations stop once the particle has either passed out of the air bearing or has impacted on the slider or the disk.

CHAPTER 5

PARTICLE MOTION NUMERICAL RESULTS

In this study, the numerical model is constructed along the centerline of the recessed region within a simple air bearing. The distance to the rail walls is far greater than the height and when combined with the small particle diameter, the effects of the wall on the particle trajectory is negligible [Zhang and Bogy 1997]. With disk velocity in the *y*-direction held at zero, the bearing pressure profile at centerline approaches that for an infinitely wide bearing. Thus gas flows in the *x*-direction are dominant. Since this study concerns only vertical and longitudinal motions of a particle, simulation can be reduced to two dimensions along a vertical plane at centerline. Also since slider length is far greater than thickness, the pressure gradient with respect to *z* is zero; thus, gas flows in the *z*-direction are zero.

The air bearing used in this study has a typical cavity depth of 3μm and a 50nm flying height. Disk speed in the *x*-direction, $\hat{U}$, was set at 20 m/s. For other pertinent parameters, refer to the appended *Mathcad* file. This *Mathcad* file is programmed to use the factored implicit scheme previously discussed. The two-dimensional pressure profile at the centerline is calculated and passed to the particle motion program, which is also enclosed as an appended *Mathcad* file. The pressure profile is plotted as *Figure 5.1.*

The particles chosen were assumed to consist of aluminum spheres with a density, ρ_p, of 4000 kg/m^3. Diameters of the particles used began at 150nm, which was incremented by 50nm for each new simulation, to a maximum particle diameter of 300nm. Since an infinite number of initial particle conditions are possible, the following parameters were used for each simulation: initial position, $X_p = 0$, $Y_p = constant$, and $Z_p = 0.5$; initial velocity in Y-direction, $V_p = 0$; initial velocity in Z-direction, $W_p = 0$.

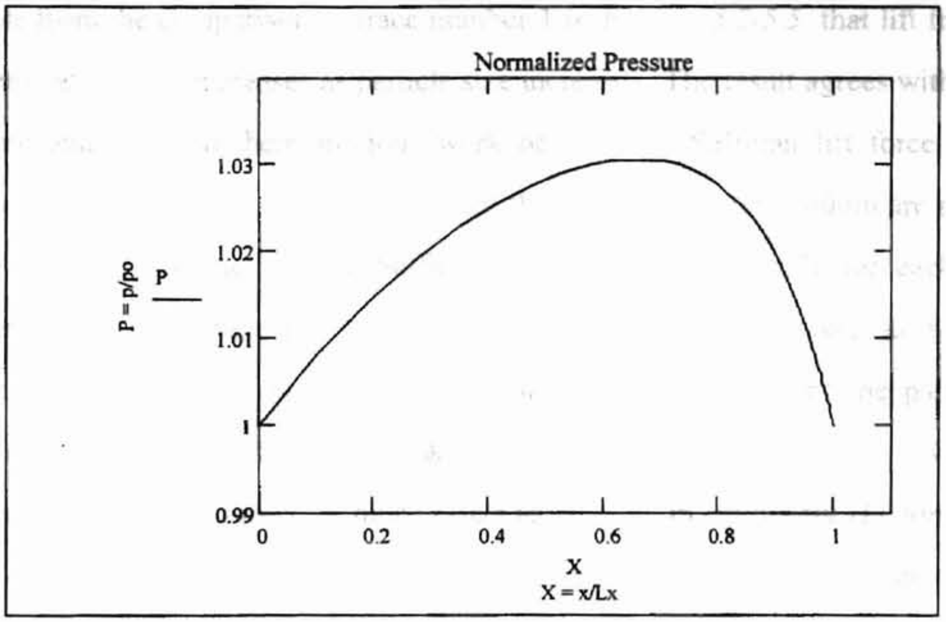

Figure 5.1. Pressure Profile at Centerline of Bearing Used in Motion Study

Initial velocity of each particle was determined by trial and error with the limitation that U_p must remain between 0.25 and 1.0 at the entrance to the bearing. Initial particle speeds slower than 0.25 or faster than 1.0 (1.0 is equal to the speed of the disk) are unlikely to occur in real world environments; therefore, although transport solutions are attainable for these numbers, they are trivial.

Several trials were run for each particle diameter, varying initial particle speed until a speed was found that allowed the particle to pass completely through the air bearing without contacting any surfaces. This initial speed was then used for each successive run for that particular particle. Additionally, initial particle speed was chosen with all particle forces present *except electrostatics*. The intent was to find an initial particle speed that would be sensitive to changes from additional forces, yet not be a contrived case. In all trial cases, excepting d = 300nm, initial particle speed was set at 1.0. For reasons yet to be discussed, initial particle speed for d = 300nm was set at 0.54.

Note from the comparison of trace number 1 in *Figures 5.2-5.5*, that lift force, with no electrostatic input, increases as particle size increases. The result agrees with findings by Zhang and Bogy in their previous work because the Saffman lift force increases according to the square of the particle radius; thus, particles below 100nm are negligibly affected. In the presence of the Saffman force, the motion study for each particle diameter began, as noted above, that precluded electrostatic force, as a baseline comparison. Electrostatic force was added in successive runs until the particle first impacted with either the slider or the disk. After the first impact was noted, several more runs were made to determine how much effect an increase in *equivalent H+ ions* made in time and *X*-direction distance to impact. One equivalent H+ ion contains the same amount of charge as one electron, or 1.602×10^{-19} Coulombs (C). The measurement of charge in equivalent H+ ions is merely a convenient method to change the electrostatic charge of the particle within the confines of a numeric program. The use of equivalent H+ ions also puts an upper bound on the amount of maximum charge the particle can acquire. Through the use of the physical constant, Bohr's radius of 5.29167×10^{-11} σm, the volume of one hydrogen atom, can be calculated. When the volume of the particle sphere is divided by the volume of one H+ ion, the maximum number of ions possible for a given diameter is the result.

Figure 5.2 is a plot of the motion study results for a particle diameter of 150nm. The first impact occurred at an equivalent H+ ion number of 11.4. This is only a fraction of the maximum possible number of H+ ions of 2.85×10^{9}. Trace number 3 impacted at H+ ions equal to 19.0 and trace number 4 impacted at H+ ions equal to 35.6. Note the electrostatic force in trace number 4 exceeded the small Saffman force and impacted the disk. The results from all studies are tabulated in *Table 5.1*.

TABLE 5.1. RESULTS FROM PARTICLE MOTION STUDY

Diameter (in nm)	Trace No.	H+ Ions	Charge (in C)
150	1	0	0
	2	11.4	1.82×10^{-18}
	3	19.0	3.04×10^{-18}
	4	35.6	5.70×10^{-18}
200	1	0	0
	2	9.6	1.54×10^{-18}
	3	16.9	2.70×10^{-18}
	4	33.7	5.41×10^{-18}
250	1	0	0
	2	1.46	2.35×10^{-19}
	3	4.39	7.04×10^{-19}
	4	13.2	2.11×10^{-18}
300	1	0	0
	2	2.28	3.65×10^{-19}
	3	20.7	3.32×10^{-18}
	4	28.5	4.56×10^{-18}

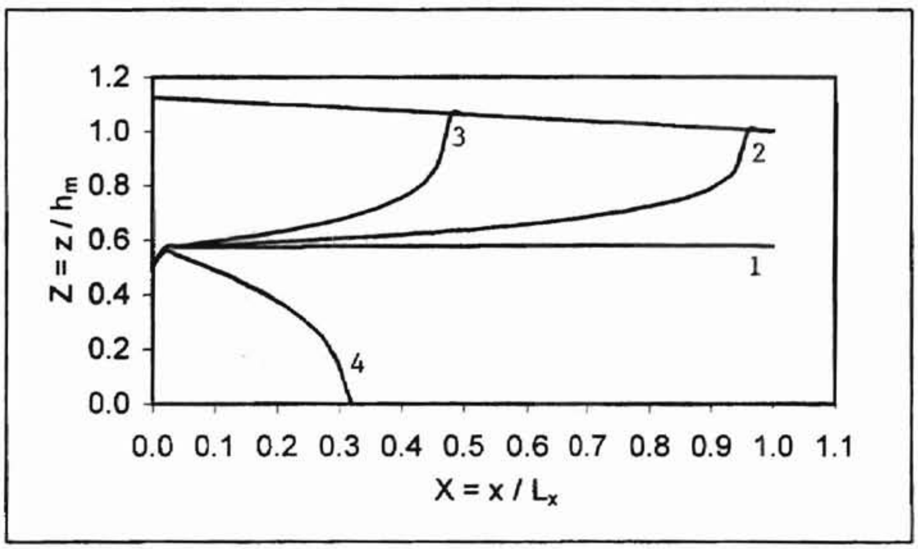

Figure 5.2. Particle Diameter 150nm: 1—No Electrostatics; 2—H+ Ions = 11.4; 3—H+ Ions = 19.0; 4—H+ Ions = 35.6

The results of the study for a particle diameter of 200nm are graphically represented in *Figure 5.3*. Initial particle speed for all runs of d = 200nm was 1.0. The first impact occurred at an equivalent H+ ion count of 9.6. Successive impacts were noted at H+ counts of 16.8 and 33.7.

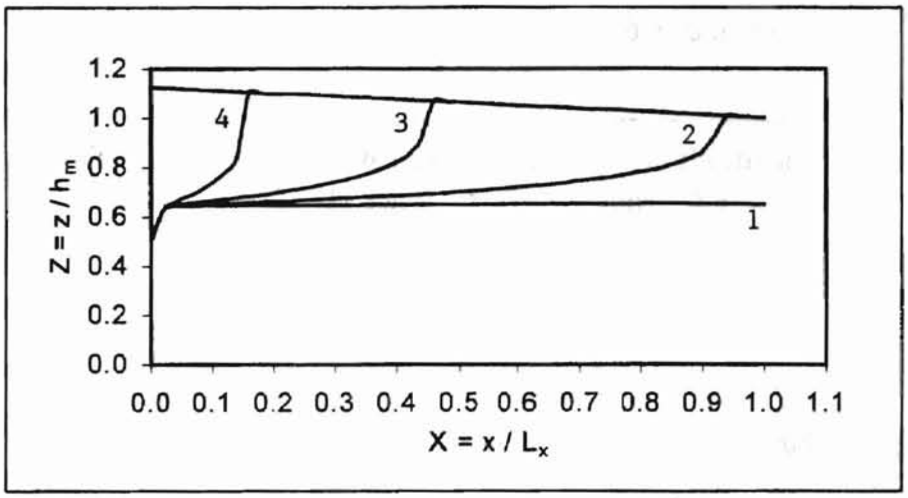

Figure 5.3. Particle Diameter 200nm: 1—No Electrostatics; 2—H+ Ions = 9.6; 3—H+ Ions = 16.9; 4—H+ Ions = 33.7

Figure 5.4 shows results from the study of a particle with a diameter of 250nm. Initial speed for all runs was also 1.0. Note the sharp upward initial swing of trace number 1. This shows the effect of the Saffman force beginning to dominate the force of drag and gravity. Note also the number of equivalent H+ ions to first impact on trace number 2 is only 1.5. This is a significant decrease. Trace number 4 impact occurred at only 13.2 equivalent H+ ions.

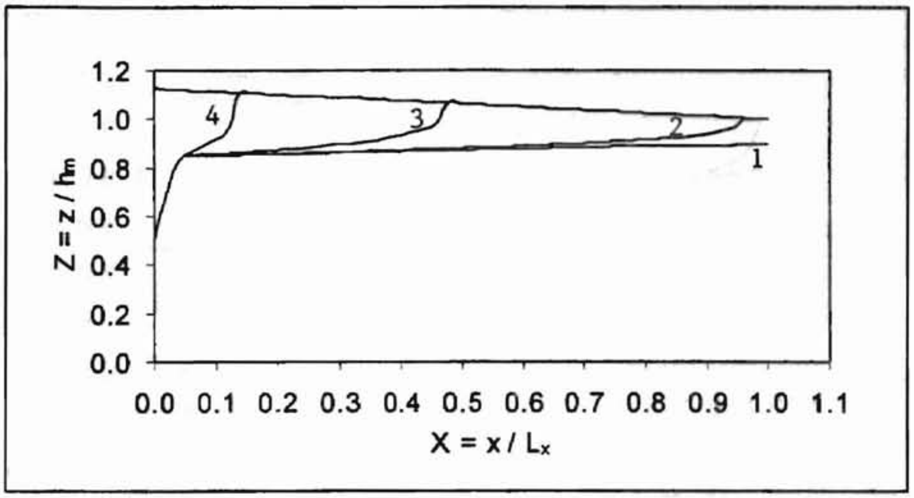

Figure 5.4. Particle Diameter 250nm: 1—No Electrostatics; 2—H+ Ion = 1.5; 3—H+ Ions = 4.4; 4—H+ Ions = 13.2

The last particle size studied has a diameter of 300nm. The results are plotted as *Figure 5.5.* At this particle size and larger, gravity and drag forces are insignificant. It was difficult to find a speed at a given height of $Z_p = 0.5$ that *did not* impact the disk of the slider. At this particle size the trajectory is very sensitive to the initial speed. Again, this agrees with the previous work of Zhang and Bogy. However, the first impact occurred at an equivalent H+ ion count of 2.3, which is slightly higher than the first impact of the particle of *Figure 5.4.* This may be due to discrepancies in the model resulting from the differing initial speed, but is more likely to be caused by the particle's increasing mass. Successive impacts occurred at H+ counts of 20.7 and 28.5. These counts too are higher than the d = 250nm particle, but note that the Saffman force has been exceeded with impact occurring on the disk.

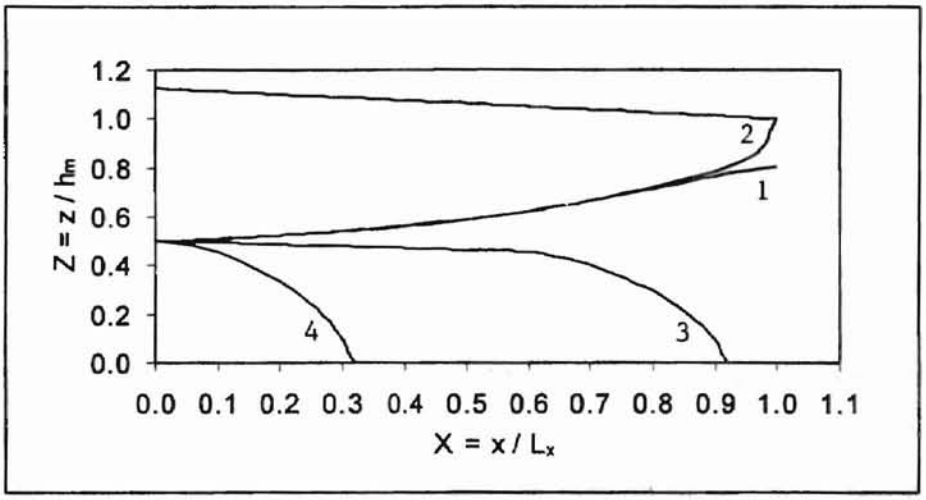

Figure 5.5. Particle Diameter 300nm: 1—No Electrostatics;
2—H+ Ions = 2.3; 3—H+ Ions = 20.7;
4—H+ Ions = 28.5

CHAPTER 6

CONCLUSIONS

With increased storage capacity of modern day electronic media, durability issues for the long-term recall of information is paramount. The formulation of the particle transport equation for electrostatic forces and the method of solution suggested in this study provide an avenue for research and design of hard disk drives. This research could benefit both hard disk drive manufacturers and the end user of the equipment with longer lasting devices. Several conclusions can be drawn from the results and data of this study:

1. Electrostatics, if present in the air bearing, can be a significant factor in the path taken by a particle. All particle trajectories through the air bearing were affected at lower charges than anticipated, which makes the findings of this study very significant. Although it can be argued, with some merit, that hard disk materials are nonconductors, only a minute charge is needed to induce a trajectory change. This small magnitude (~1.5 H+ ions, or 2.35×10^{-19} C) might be sufficient to ionize particles that exert an electrostatic force. In other words, this is equivalent to the charge carried by 1.5 electrons.
2. Electrostatic charges are very likely present at these small magnitudes. High-speed debris flows are well known to produce electrostatic charges.
3. If electrostatic forces are generated within the bearing, then there are surely instances when even fewer charges than simulated can be present. Such an amount will affect a trajectory change. The initial particle height in all trial runs was set at a conservative $Z_p = 0.5$. Trial runs conducted at initial height closer to the disk or slider have resulted in trajectory changes at some very low magnitudes.

4. It is proposed that electrostatic forces could explain why debris tends to accumulate in the cavity area. If such debris enters the cavity area on the slider, a charged particle would tend to remain.

Understanding particle path changes at very low electrical charges could be significant. In the presence of electrostatic charges in modern air bearings, contaminant control methods in the hard disk drive environment will need to be devised. What effects do oscillating charges have on particle motion? To illustrate, after writing the particle transport program, the first initial runs produced a few particle paths that oscillated between the disk and plate surfaces like a sine wave. Realizing such an event is a low probability it was discovered the routine that examined the distance *r* in the electrostatic force was reversed to select the longest dimension. This reversed the direction of the electrostatic force and produced *repulsion*. If the slider could push the particles, impact damage on the disk surface and debris accumulation on the slider could be possible.

REFERENCES

Akai, T.J. *Applied Numerical Methods for Engineers*. New York: Wiley, 1994.

Ashar, K.G. *Magnetic Disk Drive Technology: Heads, Media, Channel, Interfaces, and Integration*. New York: IEEE Press, 1996.

Berardinis, L.A. "Keeping the Drive Alive." *Machine Design* (Oct. 1995), pp. 84-95.

Bhushan, B., Ed. *Tribology and Mechanics of Magnetic Storage Devices*. New York: Springer-Verlag, 1990.

Burgdorfer, A. "The Influence of the Molecular Mean Free Path on the Performance of Hydrodynamic Gas Lubricated Bearings." *ASME Journal of Basic Engineering*. (March 1959), pp. 94-100.

Cameron, A. *Basic Lubrication Theory*. 3rd Edition. New York: Wiley, 1981.

Castelli, V. and J. Pirvics. "Review of Numerical Methods in Gas Bearing Film Analysis." *Journal of Lubrication Technology* (Oct. 1968), pp. 778-792.

Cercignani, C. and C.D. Pagani. "Variational Approach to Boundary-Value Problems in Kinetic Theory." *Physics of Fluids*, Vol. 9, No. 6 (June 1966), pp. 1167-1173.

Cha, E. and D.B. Bogy. "A Numerical Scheme for Static and Dynamic Simulation of Subambient Pressure Shaped Rail Sliders." *Journal of Tribology*, Vol. 117 (Jan. 1995), pp. 36-46.

Coleman, R. "The Numerical Solution of Linear Elliptic Equations." *Journal of Lubrication Technology* (Oct. 1968), pp. 773-776.

Corson, D.R. and P. Lorrain. *Introduction to Electromagnetic Fields and Waves*. San Francisco: W. H. Freeman and Company, 1962.

DiPrima, R.C. "Asymptotic Method for an Infinitely Long Slider Squeeze-Film Bearing." *Journal of Lubrication Technology* (Jan. 1968), pp. 173-183.

Fukui, S. and R. Kaneko. "A Database for Interpolation of Poiseuille Flow Rates for High Knudsen Number Lubrication Problems." *Transactions of the ASME*, Vol. 112 (Jan. 1990), pp. 78-83.

Fukui, S. and R. Kaneko. "Analysis of Ultra-Thin Gas Film Lubrication Based on Linearized Boltzmann Equation: First Report—Derivation of a Generalized Lubrication Equation Including Thermal Creep Flow." *Journal of Tribology*, Vol. 110 (Apr. 1988), pp. 253-262

Gans, R.F. "Lubrication Theory at Arbitrary Knudsen Number." *Journal of Tribology*, Vol. 107 (1984), pp. 431-433.

Gross, W.A., L.A. Matsch, V. Castelli, A. Eshel, J.H. Vohr, and M. Wildmann. *Fluid Film Lubrication*. New York: Wiley, 1980.

Hiller B. and G.P. Singh. "Interaction of Contamination Particles With the Particulate Slider/Disk Interface." *Advanced Information Storage Systems*, Vol. 173, No. 2, 1991.

Holman, J.P. *Heat Transfer*. 3rd Edition. New York: McGraw-Hill, 1972.

Hsia, Y.-T. and G.A. Domoto. "An Experimental Investigation of Molecular Rarefaction Effects in Gas Lubricated Bearings at Ultra-Low Clearances." *Transactions of the ASME*, Vol. 105 (Jan. 1983), pp. 120-130.

Hu, Y. and D.B. Bogy. "Dynamic Stability and Spacing Modulation of Sub-25nm Fly Height Sliders." *Journal of Tribology*, Vol. 119 (Oct. 1997), pp. 646-652.

Hu, Y. and D.B. Bogy. "Solution of the Rarefied Gas Lubrication Equation Using an Additive Correction-Based Multigrid Control volume Method." *Transactions of the ASME*, Vol. 120 (April 1998), pp. 280-288.

Koka, R. and A.R. Kumaran. "Visualization and Analysis of Particulate Buildup on the Leading Edge Taper Sliders." *Advanced Information Storage Systems*, Vol. 161, No. 2 (1991).

Kreyszig, E. *Advanced Engineering Mathematics*. 7th Edition. New York: Wiley, 1993.

Liu, V.C., S.C. Pang, and H. Jew. "Sphere Drag in Flows of Almost-Free Molecules." *Physics of Fluids*, Vol. 8, No. 5 (1965), pp. 788-796.

Saffman, P.G. "The Life on a Small Sphere in a Slow Shear Flow." *Journal of Fluid Mechanics*, Vol. 22, Pt. 2 (1965), pp. 385-400.

Tokuyama, M. and H. Shinichi. "Dynamic Flying Characteristics of Magnetic Head Slider With Dust." *Journal of Tribology*, Vol. 116 (Jan. 1994), pp. 95-100.

Vohr, J.H. "Numerical Methods in Hydrodynamic Lubrication." *CRC Handbook of Lubrication*, Vol. 2 (1970), pp. 93-104.

White, J.W. and A. Nigam. "A Factored Implicit Scheme for the Numerical Solution of the Reynolds Equation at Very Low Spacing." *Transactions of the ASME*, Vol. 102 (Jan. 1980), pp. 80-85.

Williams, J.A. *Engineering Tribology*. New York: Oxford University Press, 1994.

Zhang, S. and D.B. Bogy. "Effects of Lift on the Motion of Particles in the Recessed Regions of a Slider." *Physics of Fluids*, Vol. 9 (May 1997), pp. 1265-1272.

Zhang, S. and D.B. Bogy. "Slider Designs for Controlling Contamination." *Journal of Tribology*, Vol. 119 (July 1997), pp. 537-540.

APPENDIX

FIS Air Bearing Pressure Profile Program

Constant and Variable Definitions

$\mu := 18 \cdot 10^{-6}$

$\lambda := 6.603777 \cdot 10^{-8}$

$p_o := 101000$

$h_m := 3050 \cdot 10^{-9}$

$\alpha := 0.00015$

$V_x := 20$

$L_x := 0.00254$

$\Delta x_{min} := 0.00000127$

$GM := 1.112$

$\Delta t := 0.000005$

$Xgrid := 52$

The constant 'a', used repeatedly in the routines that follow:

$$a := \frac{\Delta t}{24 \cdot \mu} \qquad a = 0.011574074074$$

$$\Lambda := \frac{6 \cdot \mu \cdot V_x \cdot L_x}{p_o \cdot \left(50 \cdot 10^{-9}\right)^2} \qquad \Lambda = 21728.317$$

<===== This bearing number is based on the flying height at the trailing edge of the rails.

NOTE: In this program, the matrices holding parameters that do have valid values on the boundaries, i.e. 'h' and 'Z', will be *indexed* from 0 to Xgrid-1. *(In other words if you have 52 valid values to put in the matrix, the indices will run from 0 to 51 (Xgrid-1) for a total of 52 positions.)* The matrices that have no valid values on the boundaries, i.e. Zx,Zxx, the corresponding constants A1 through D3, the linear operator-L1, ϕ, ΔZ, and ΔZ^*, are *indexed* from 0 to Xgrid-2 valid entries. *(Following the above example, if a previous matrix had 52 valid entries and a new matrix was built from the old one with invalid boundaries on the upper and lower, the new matrix would be indexed from 0 to 50 with valid entries in 1 to 50. The values for position'0" would not be defined and Mathcad would put a 0 in that position.)* This is one good thing about MathCad--it allows you to define a Matrix at any sequence of indices desired and will automatically put zeroes in undefined positions. The matrix size would automatically be set to the value of the largest index used. Using the previous stated scheme allows the interior matrices and the primary matrices to reference the same position with the same set of index counters. For instance, we currently have height, 'h', with 52 by 1 valid entries. This matrix would be indexed from rows 0 to 51 and only one column, 0. The derivative, 'Zx', is not defined on the boundaries and would be indexed from 0 to 50 with defined values in 1 to 50. Undefined values for indices containing a 0 would be left undefined and Mathcad would insert zeroes as placeholders.

THE PROGRAM BEGINS:

The grid spacing matrix:

$$x := \left| \begin{array}{l} tmp_{Xgrid-1} \leftarrow L_x \\ tmp_0 \leftarrow 0 \\ \text{for } i \in (Xgrid-2) .. 1 \\ \quad tmp_i \leftarrow tmp_{i+1} - \Delta x_{min} \cdot GM^{(Xgrid-i-2)} \\ tmp \end{array} \right.$$

Here is the matrix for the height,
based on the formula for a line y=mx + b:

$m := -\tan(\alpha)$ $\quad m = -0.000150000001$

$b := h_m - m \cdot L_x$ $\quad b = 3.431000002858 \cdot 10^{-6}$

$$h := \left| \begin{array}{l} \text{for } i \in 0 .. Xgrid-1 \\ \quad tmp_i \leftarrow m \cdot x_i + b \\ tmp \end{array} \right.$$

x =

0.002501214478
0.00250626302
0.002510803075
0.002514885859
0.002518557427
0.002521859197
0.002524828415
0.002527498574
0.002529899797
0.00253205917
0.002534001052
0.002535747349
0.00253731776
0.00253873

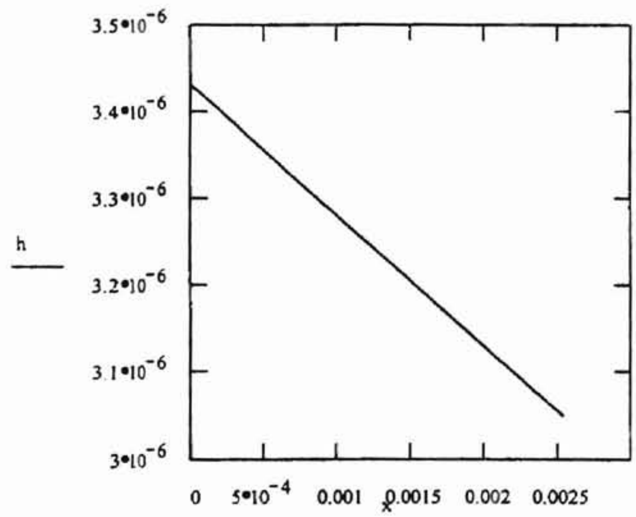

h =

$3.4310000029 \cdot 10^{-6}$
$3.3917908668 \cdot 10^{-6}$
$3.3571945745 \cdot 10^{-6}$
$3.3260828008 \cdot 10^{-6}$
$3.2981045871 \cdot 10^{-6}$
$3.2729443229 \cdot 10^{-6}$
$3.2503181861 \cdot 10^{-6}$
$3.2299709407 \cdot 10^{-6}$
$3.2116730582 \cdot 10^{-6}$
$3.1952181279 \cdot 10^{-6}$
$3.1804205286 \cdot 10^{-6}$
$3.1671133351 \cdot 10^{-6}$
$3.1551464345 \cdot 10^{-6}$
$3.1443848331 \cdot 10^{-6}$

rows(h) = 52 $\quad$ cols(h) = 1

Loading the 'p' and 'Z' matrices with initial guesses:

$$p := \left| \begin{array}{l} \text{for } i \in 0 .. Xgrid - 1 \\ \quad tmp_i \leftarrow p_0 \\ tmp \end{array} \right.$$

$$Zz := \overrightarrow{(p \cdot h)}$$

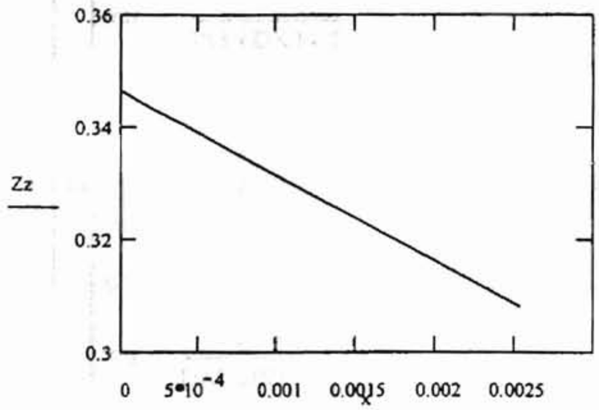

The matrix 'Z' is = p*h and is defined on the boundaries, therefore its *size* is (Xgrid-1 x 1). Its *indices* run from 0 to Xgrid-1 and 0.

Zz =

0.346531000289
0.342570877551
0.339076652025
0.335934362882
0.333108563293
0.330567376612
0.328282136791
0.32622706501
0.324378978876
0.322717030913
0.321222473393
0.319878446846
0.31866978988
0.317582868147
0.316605420546
0.315726420904
0.314935953601
0.314225101709
0.313585846411

rows(Zz) = 52

cols(Zz) = 1

Defining the constants, A1, A2, A3, C1, C2, and C3.

$$A1 := \left| \begin{array}{l} \text{for } i \in 1..\, Xgrid - 2 \\ \quad \left| \begin{array}{l} DX1 \leftarrow x_{i+1} - x_i \\ DX0 \leftarrow x_i - x_{i-1} \\ tmp_i \leftarrow \dfrac{2}{DX1 \cdot (DX0 + DX1)} \end{array} \right. \\ tmp \end{array} \right.$$

$$C1 := \left| \begin{array}{l} \text{for } i \in 1..\, Xgrid - 2 \\ \quad \left| \begin{array}{l} DX1 \leftarrow x_{i+1} - x_i \\ DX0 \leftarrow x_i - x_{i-1} \\ tmp_i \leftarrow \dfrac{DX0}{DX1 \cdot (DX1 + DX0)} \end{array} \right. \\ tmp \end{array} \right.$$

$$A2 := \left| \begin{array}{l} \text{for } i \in 1..\, Xgrid - 2 \\ \quad \left| \begin{array}{l} DX1 \leftarrow x_{i+1} - x_i \\ DX0 \leftarrow x_i - x_{i-1} \\ tmp_i \leftarrow \dfrac{-2}{DX0 \cdot DX1} \end{array} \right. \\ tmp \end{array} \right.$$

$$C2 := \left| \begin{array}{l} \text{for } i \in 1..\, Xgrid - 2 \\ \quad \left| \begin{array}{l} DX1 \leftarrow x_{i+1} - x_i \\ DX0 \leftarrow x_i - x_{i-1} \\ tmp_i \leftarrow \dfrac{DX1 - DX0}{DX1 \cdot DX0} \end{array} \right. \\ tmp \end{array} \right.$$

$$A3 := \left| \begin{array}{l} \text{for } i \in 1..\, Xgrid - 2 \\ \quad \left| \begin{array}{l} DX1 \leftarrow x_{i+1} - x_i \\ DX0 \leftarrow x_i - x_{i-1} \\ tmp_i \leftarrow \dfrac{2}{DX0 \cdot (DX1 + DX0)} \end{array} \right. \\ tmp \end{array} \right.$$

$$C3 := \left| \begin{array}{l} \text{for } i \in 1..\, Xgrid - 2 \\ \quad \left| \begin{array}{l} DX1 \leftarrow x_{i+1} - x_i \\ DX0 \leftarrow x_i - x_{i-1} \\ tmp_i \leftarrow \dfrac{-DX1}{DX0 \cdot (DX1 + DX0)} \end{array} \right. \\ tmp \end{array} \right.$$

$\text{rows}(A1) = 51$ $\quad \text{cols}(A1) = 1$ $\quad \text{rows}(C1) = 51$ $\quad \text{cols}(C1) = 1$

$\text{rows}(A2) = 51$ $\quad \text{cols}(A2) = 1$ $\quad \text{rows}(C2) = 51$ $\quad \text{cols}(C2) = 1$

$\text{rows}(A3) = 51$ $\quad \text{cols}(A3) = 1$ $\quad \text{rows}(C3) = 51$ $\quad \text{cols}(C3) = 1$

The 'Z' derivatives are written as functions so they can be repeatedly called from inside a loop. They do not exist at the boundaries.

$$Zx(i,Z) := C1_i \cdot Z_{i+1} + C2_i \cdot Z_i + C3_i \cdot Z_{i-1}$$

$$Zxx(i,Z) := A1_i \cdot Z_{i+1} + A2_i \cdot Z_i + A3_i \cdot Z_{i-1}$$

The matrix 'PHI' is written as a function so it can be repeatedly called from inside a loop. It does not exist at the boundaries.

$$PHI(i,Z) := 2 \cdot a \cdot \left[\left(Z_i + 6 \cdot \lambda \cdot p_o \right) \cdot Zxx(i,Z) \cdot h_i - Zx(i,Z) \cdot \left(Z_i \cdot m - Zx(i,Z) \cdot h_i \right) - 6 \cdot \mu \cdot V_x \cdot Zx(i,Z) \right]$$

The matrix 'L1' is written as a function so it can be repeatedly called from inside a loop. It does not exist at the boundaries.

$$\Gamma1(i,Z) := a \cdot \left[\left(2 \cdot h_i \cdot Zx(i,Z) - Z_i \cdot m - 6 \cdot \mu \cdot V_x \right) \cdot C3_i + \left(Z_i + 6 \cdot \lambda \cdot p_o \right) \cdot h_i \cdot A3_i \right]$$

$$\Gamma2(i,Z) := a \cdot \begin{bmatrix} h_i \cdot Zxx(i,Z) - m \cdot Zx(i,Z) + \left(2 \cdot h_i \cdot Zx(i,Z) - Z_i \cdot m - 6 \cdot \mu \cdot V_x \right) \cdot C2_i \ldots \\ + \left(Z_i + 6 \cdot \lambda \cdot p_o \right) \cdot h_i \cdot A2_i \end{bmatrix} - 1$$

$$\Gamma3(i,Z) := a \cdot \left[\left(2 \cdot h_i \cdot Zx(i,Z) - Z_i \cdot m - 6 \cdot \mu \cdot V_x \right) \cdot C1_i + \left(Z_i + 6 \cdot \lambda \cdot p_o \right) \cdot h_i \cdot A1_i \right]$$

$\Gamma1(50, Zz) = 6496.791875368938$

$\Gamma2(50, Zz) = -13702.11829193635$

$\Gamma3(50, Zz) = 7204.32639026533$

These matrices are based on the constants A1, A2, A3, C1, C2, and C3. An index at i=0 will return a zero value but it is not a valid result. 1 to Xgrid-2 are valid 'i' indeces and correspond to the interior of the slider.

Routine to assemble the tridiagonal matrix. This matrix has size (Xgrid-2) by (Xgrid-2).

```
L1MAT(Z) := | tmp[0,0] ← Γ2(1,Z)
            | tmp[0,1] ← Γ3(1,Z)
            | tmp[Xgrid-3, Xgrid-4] ← Γ1(Xgrid - 2, Z)
            | tmp[Xgrid-3, Xgrid-3] ← Γ2(Xgrid - 2, Z)
            | for i ∈ 1 .. Xgrid - 4
            |     | tmp[i,i-1] ← Γ1(i + 1, Z)
            |     | tmp[i,i] ← Γ2(i + 1, Z)
            |     | tmp[i,i+1] ← Γ3(i + 1, Z)
            | tmp
```

The statement below is just a trial to make sure the function routine is working. Note the size is square with (Xgrid-2) length.

$L1 := L1MAT(Zz)$

$rows(L1) = 50$

$cols(L1) = 50$

```
φMAT(Z) := | for i ∈ 0 .. Xgrid - 3
           |     tmp[i] ← -1·PHI(i + 1, Z)
           | tmp
```

This routine is a function that assembles the column matrix, PHI, to use in the matrix math solution for ΔZ.

$Toll := 0.0005$ <===== This is the parameter to stop the iterations as ΔZ approaches zero. It is global and is automatically recognized by the routine below

This routine sets up a loop that solves the linear operators L1 and L2. It then updates Z, calculates new L1 and phi and solves them again. The routine is continued until the counter reaches the value of Tsteps or the change in Z is within tolerance.

```
Z_f(Tsteps, Zz) := | Z ← Zz
                   | for Loop ∈ 1 .. Tsteps
                   |    | oldZ ← Z
                   |    | ΔZ ← L1MAT(Z)^-1 · φMAT(Z)
                   |    | for i ∈ 1 .. Xgrid − 2
                   |    |    Z_i ← oldZ_i + ΔZ_(i−1)
                   |    | break if max(ΔZ) < Toll
                   | Z
```

```
Loop(Tsteps, Zz) := | Z ← Zz
                    | for Loop ∈ 1 .. Tsteps
                    |    | oldZ ← Z
                    |    | ΔZ ← L1MAT(Z)^-1 · φMAT(Z)
                    |    | for i ∈ 1 .. Xgrid − 2
                    |    |    Z_i ← oldZ_i + ΔZ_(i−1)
                    |    | break if max(ΔZ) < Toll
                    | Loop
```

Since it was discovered that the program just took a few seconds to iterate to conversion, this routine is basically a copy of the solution routine above with the exception of a new name and the last line where instead of an output of 'Z' this routine returns an output of the counter, 'Loop'. Its mainly just an FYI item to find out the number of iterations it took to converge.

$Tsteps := 30$ <===== Defining 'Tsteps' and 'Z_{final}' this way makes it easier to change the # of iterations in both 'Z_{final}' and 'Loop'.

$Z_{final} := Z_f(Tsteps, Zz)$ <===== Z_{final} ( ) now contains the solutions for the converged system.

$rows(Z_{final}) = 52$

$cols(Z_{final}) = 1$

$max(Z_{final}) = 0.346531000289$

$Loop(Tsteps, Zz) = 15$ <===== This is the the number of iterations the solution took to converge.

$$P := \overrightarrow{\left(\frac{Z_{final}}{h}\right)} \cdot \frac{1}{p_o}$$ <===

This is a Mathcad operation known as a "vectorized" operation. It takes every element in Z_{final} and divides it by the corresponding element in h. This matix result is multiplied by the scalar, $1/p_o$, to give the final result as a vector of normalized pressures.

$\max(P) = 1.030637$ <===

The operation, max( ), is a built in Mathcad function that searches through all the elements of the specified matrix and returns the largest element.

$\text{rows}(P) = 52$

$\text{cols}(P) = 1$

$$X := \frac{x}{L_x}$$ <===

White and Nigam do not use a normalized 'X' until they plot the final result. Here the x-values are normalized or made 'non-dimensional' by dividing by the length in x, L_x.

$\text{rows}(X) = 52$

$\text{cols}(X) = 1$

$\max(P) = 1.030636653612$

The normalized pressure plot.

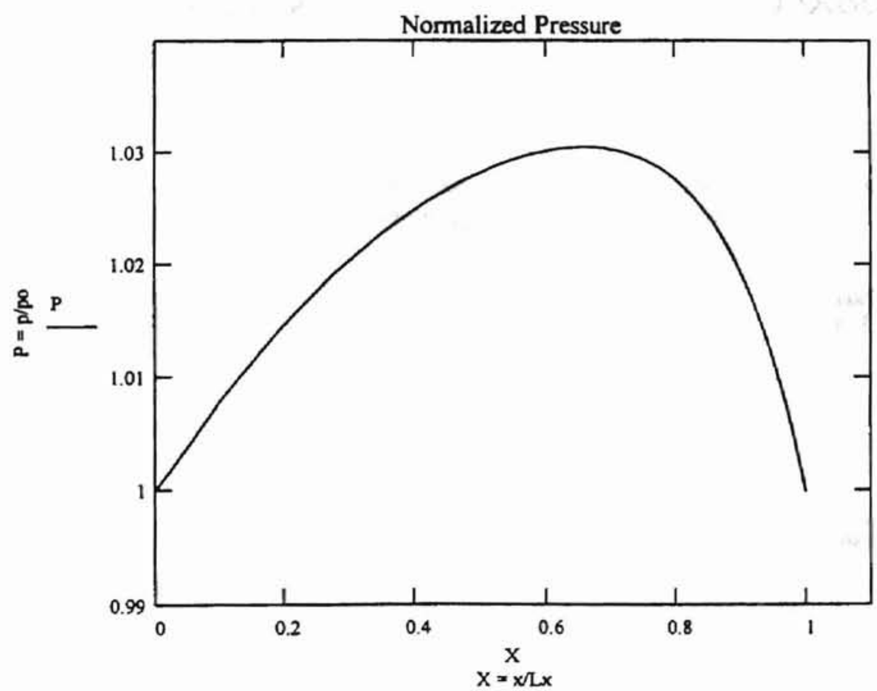

The following are files that are written to MS Excel files for the next program (the particle transport program) to read.

$$\text{Param} := \begin{bmatrix} \mu \\ \lambda \\ p_o \\ h_m \\ \alpha \\ V_x \\ \text{Xgrid} \\ L_x \\ \Delta x_{min} \\ GM \\ \Delta t \end{bmatrix}$$

Param =

0.000018
$6.603777 \cdot 10^{-8}$
101000
$3.05 \cdot 10^{-6}$
0.00015
20
52
0.00254
$1.27 \cdot 10^{-6}$
1.112
$5 \cdot 10^{-6}$

The input parameters are written in the order as defined by the statement on the left. Below is the Mathcad 'component' to write to a file.

D:\Param.xls

Param

The normalized vector for X was defined above. Here it is printed to a file.

D:\Xout.xls

X

$$H := \frac{h}{h_m}$$

White and Nigam do not use a normalized 'H'. Here the h-values are normalized or made 'non-dimensional' by dividing by the minimum height, h_m.

rows(H) = 52

cols(H) = 1

D:\H.xls

H

The normalized vector for P was defined above. Here it is printed to a file.

D:\Pout.xls

P

Particle Motion Study

Constant and Variable Definitions

Pars :=

D:\Param.xls

Reading in the problem parameters and geometry.

X :=

D:\Xout.xls

rows(X) = 52

rows(Pars) = 11

$\mu := Pars_0$ $\mu = 0.000018$

$\lambda := Pars_1$ $\lambda = 6.603777 \cdot 10^{-8}$

$p_o := Pars_2$ $p_o = 101000$

$h_m := Pars_3$ $h_m = 3.05 \cdot 10^{-6}$

$\alpha := Pars_4$ $\alpha = 0.00015$

$V_x := Pars_5$ $V_x = 20$

$Xgrid := Pars_6$ $Xgrid = 52$

$L_x := Pars_7$ $L_x = 0.00254$

$\Delta x_{min} := Pars_8$ $\Delta x_{min} = 1.27 \cdot 10^{-6}$

$GM := Pars_9$ $GM = 1.112$

H :=

D:\H.xls

rows(H) = 52

P :=

D:\Pout.xls

rows(P) = 52

Note: the above reads the pressure profile and air bearing parameters from the program, 'white_1D.MCD'.

P =

1
1.0081708535
1.0144399393
1.0192608987
1.0229134871
1.0256388183
1.0276293816

X =

0.9847301094
0.9867177243
0.9885051478
0.990112543
0.9915580422
0.9928579516
0.9940269349

H =

1.1249180337
1.1120625793
1.1007195326
1.0905189511
1.0813457662
1.0730964993
1.0656780938

rows(P) = 52

rows(X) = 52

rows(H) = 52

$vs := cspline(X, P)$ The function 'PanyX( )' returns the pressure at any non-dimensional X value.

$PanyX(X_{in}) := interp(vs, X, P, X_{in})$ PanyX(0.824) = 1.0263892615

PanyX(.999) = 1.0002865047 $ii := 0, 0.001 .. 1$

$Ppoints := Xgrid \cdot 100$ $Ppoints = 5200$

$$XX := \left| \begin{array}{l} \text{for } i \in Ppoints..0 \\ \quad tmp_i \leftarrow \dfrac{i}{Ppoints} \\ tmp \end{array} \right.$$

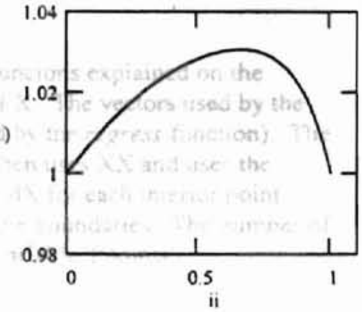

$$Px := \left| \begin{array}{l} tmp_0 \leftarrow 0 \\ tmp_{Ppoints} \leftarrow 0 \\ \text{for } i \in 1..Ppoints - 1 \\ \quad tmp_i \leftarrow \dfrac{PanyX(XX_{i+1}) - PanyX(XX_{i-1})}{XX_{i+1} - XX_{i-1}} \\ tmp \end{array} \right.$$

The function 'PanyX( )' is based on the Mathcad intrinsic function *interp( )* and *regress( )*. In generic terms, the *regress* function inputs an vector to *interp* based on an 'n[th]' order polynomial--its arguments are *regress(x,y,n)*. The *interp* function uses the same x and y values as *regress* plus the vector returned by *regress* to interpolate a y-value, given any valid x in the same range as the input vector for x. In this case, *regress* is evaluating input X and P values read from the plot in Z&B's paper and recreates the plot so I can get a value for pressure in the air bearing at any value of X.

$rows(Px) = 5201$ $\quad vp := cspline(XX, Px)$

$$dPdX(X_{in}) := interp(vp, XX, Px, X_{in})$$

$$dPdX(0.9997) = -0.2991679996$$

Px =	XX =
0	0
0.08452	0.00019
0.0845	0.00038
0.08448	0.00058
0.08446	0.00077
0.08445	0.00096
0.08443	0.00115
0.08441	0.00135
0.08439	0.00154
0.08437	0.00173
0.08435	0.00192
0.08433	0.00212
0.08432	0.00231
0.0843	0.0025
0.08428	0.00269

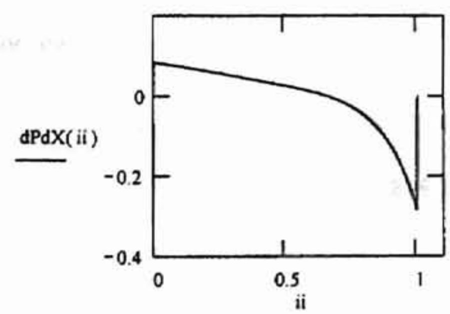

$rows(Px) = 5201$ $\quad rows(XX) = 5201$

dPdX( ) is now a function using the same Mathcad intrinsic funcions explained on the previous page and returns a value dP/dX at any given value of X. The vectors used by the *interp* and *regress* funtions are XX, Px, and vp (vp is returned by the *regress* function). The vector XX fills a vector with non-dimensional X values. Px then uses XX and uses the central difference method to fill a vector with estimates of dP/dX for each interior point. The values of the gradient of P in X is assumed to be zero at the boundaries. The number of points in the vectors XX and Px is arbitrary and is set by the variable 'Ppoints'.

$\mathrm{PanyX}(0.824) = 1.0263892615$	<=====	Now, values for Pressure at any X is returned by the function routine 'PanyX(X-value)'. Likewise the value of the first derivative of Pressure with respect to X, also at any X, is returned by the funtion routine 'dPdX(X-value)'.
$\mathrm{dPdX}(0.824) = -0.0622170931$	<=====	

Note: all lengths are in meters.

$h_m := \mathrm{Pars}_3$	slider height at trailing edge	$h_m = 3.05 \cdot 10^{-6}$
$\alpha := \mathrm{Pars}_4$	angle of slider	$\alpha = 0.00015$
$\lambda := \mathrm{Pars}_1$	molecular mean free path	$\lambda = 6.603777 \cdot 10^{-8}$
$U_{hat} := \mathrm{Pars}_5$	disk speed in x-direction, in m/sec	$U_{hat} = 20$
$V_{hat} := 0$	disk speed in y-direction	
$\mathrm{diam}_{disk} := 0.100$	disk diameter at slider position, in m	
$\Omega_{hat} := \dfrac{U_{hat}}{\pi \cdot \mathrm{diam}_{disk}}$	rotational speed of disk, in revolutions/sec (RPS)	$\Omega_{hat} = 63.66$ in RPS
	or	$\Omega_{hat} \cdot 60 = 3819.7$ in RPM
$L_o := \mathrm{Pars}_7$	length of slider	$L_o = 0.00254$
$Kn_h := \dfrac{\lambda}{h_m}$	Knudsen number related to minimum height	$Kn_h = 0.0216517279$
$\rho_g := 1.23$	density of air at 71° F, in kg/m³	
$\mu_g := \mathrm{Pars}_0$	dynamic viscosity of air at 71° F, in Pa*sec	$\mu_g = 0.000018$
$\nu_g := \dfrac{\mu_g}{\rho_g}$	kinematic viscosity of air at 71° F, m²/sec	$\nu_g = 1.46 \cdot 10^{-5}$

$p_o := Pars_2$ atmospheric pressure, in Pa $p_o = 101000$

$Re_h := \frac{U_{hat} \cdot h_m}{\nu_g}$ Renolds number based on the minimum height. $Re_h = 4.1683333333$

$R_L := \frac{U_{hat}}{\Omega_{hat} \cdot L_o}$ non-dimensional number used in the differential equations for particle motion

$R_L = 123.6847501413$

$R_h := \frac{U_{hat}}{\Omega_{hat} \cdot h_m}$ non-dimensional number used in the differential equations for particle motion

$R_h = 103003.03782$

$R_g := 287$ gas constant, in J/kg/ºK

$\rho_p := 4000$ particle density, in kg/m³

$T_g := 294$ characteristic temperature of gas (71ºF in Kelvin)

$T_p := 294$ characteristic temperature of particle wall, assumed to equal that of the gas

$d := 250 \cdot 10^{-9}$ particle sphere diameter

$D_p := \frac{d}{h_m}$ non-dimensional sphere diameter $D_p = 0.08197$

$Kn_d := \frac{\lambda}{d}$ Knudsen number related to the particle sphere diameter $Kn_d = 0.26415108$

$g_z := 9.81$ acceleration of gravity, in m/s²

Slider geometry.

$x := X \cdot L_o$ from Z&B"s paper, there are 'Xnodes' entries in 'x', from 0 to (Xnodes-1).

The height is based on the minimum height and slider angle.
The geometry is calculated using the formula for a line, $y=mx+b$
where 'm' is the slope and 'y' is the y-intercept. At $x=L_o$, $y=h_m$, solve for b.

$m := -\tan(\alpha)$ $m = -0.00015$ $b := h_m - m \cdot L_o$ $b = 3.431 \cdot 10^{-6}$ $\frac{b}{h_m} = 1.124918$

$H(Xvalue) := \frac{m \cdot (Xvalue - L_o) + b}{h_m}$ H( ) is a function that calculates a value of the non-dimensional height, 'H', given a value of the non-dimensional position in X.

$H(0) = 1.1249180337$

$H(0.346) = 1.0816963941$

Gas velocity in x-dir., U_g.

$$Vel_{prefix} := \frac{p_o}{2 \cdot \rho_g \cdot U_{hat}^2} \cdot \frac{h_m}{L_o} \cdot Re_h$$

$Vel_{prefix} = 0.5137535542$ This is a constant used in the formulas for U_g and V_g.

$$U_g(X_{in}, Z) := Vel_{prefix} \cdot dPdX(X_{in}) \cdot \left(Z^2 - Z \cdot H(X_{in}) - Kn_h \cdot H(X_{in})\right) + \left(1 - \frac{Kn_h + Z}{2 \cdot Kn_h + H(X_{in})}\right)$$

$U_g(0, 1.1) = 0.0398638118$

$U_g(1, 1) = 0.0207530491$

$U_g(\ )$ is a function for velocity of gas in X-direction. The arguments for dPdX( ) and H( ) are used at the same value of X. $U_g(\ )$ itself uses the arguments U_g(input X value, Particle height).

Motion equation function routines.

$$k(X_{in}, Z) := \left| \frac{U_{hat}}{h_m} \cdot \left[Vel_{prefix} \cdot dPdX(X_{in}) \cdot (2 \cdot Z - H(X_{in})) - \frac{1}{2 \cdot Kn_h + H(X_{in})} \right] \right|$$

$k(0, 0.5) = 5.61313 \cdot 10^6$ The function, k( ), is used in the Saffman lift force equation.

$$Sdata := \begin{bmatrix} 1 & .9 & .8 & .7 & .6 & .5 & .4 & .3 & .2 & .1 & .01 & .00001 \\ 0.148 & 0.152 & 0.154 & 0.156 & 0.155 & 0.154 & 0.153 & 0.151 & 0.150 & 0.150 & 0.149 & 0.149 \end{bmatrix}$$

```
β(S) := | cnt ← 10
        | error("S out of range.")  if (S<Sdata[0,11]) + (S>Sdata[0,0])
        | while cnt≥0
        |    | break  if [(S≤Sdata[0,cnt])·(S≥Sdata[0,cnt+1])]
        |    | cnt ← cnt − 1
        | tmp ← Sdata[1,cnt+1] + ((S − Sdata[0,cnt+1]) / (Sdata[0,cnt] − Sdata[0,cnt+1]))·(Sdata[1,cnt] − Sdata[1,cnt+1])  otherwise
        | tmp
```

'β(S)' is a linear interpolation routine to pull the proper value out of 'Sdata'. The routine is called by the funtion for the coefficient of drag, which follows.

$$C_d(Ug, Up, Wp) := \left| \begin{array}{l} S \leftarrow \dfrac{\sqrt{(U_{hat} \cdot Ug - U_{hat} \cdot Up)^2 + (U_{hat} \cdot Wp)^2}}{\sqrt{2 \cdot R_g \cdot T_g}} \\ cnt \leftarrow 0 \\ \text{while } cnt < 1 \\ \quad \left| \begin{array}{l} tmp \leftarrow 346355 \\ \text{break if } S < 0.00001 \\ C_{dfm} \leftarrow \dfrac{2}{S^3} \left[\dfrac{4 \cdot S^4 + 4 \cdot S^2 - 1}{4 \cdot S} \cdot \mathrm{erf}(S) + \dfrac{e^{\frac{-S^2}{2}}}{\sqrt{\pi}} \cdot (S^2 + 0.5) \right] + \dfrac{2}{3} \cdot \dfrac{\sqrt{\pi}}{S} \cdot \sqrt{\dfrac{T_p}{T_g}} \\ tmp \leftarrow C_{dfm} \cdot \left(1 - \dfrac{\beta(S)}{Kn_d} \right) \\ cnt \leftarrow cnt + 1 \end{array} \right. \\ tmp \end{array} \right.$$

This is a formulation for calculating the coefficient of drag for a sphere in a flow that is almost free of molecules, i.e., a rarefied gas. The parameter, 'S' and the function $\beta(S)$ are given in a paper by Liu (1965). They are used to calculate the C_d. The function is set to return a C_d of 346,355 if 'S' approaches zero and either goes out of the defined range for the function '$\beta(S)$' or tries to divide by zero in the calculation of C_{dfm}. This function returns a larger and larger value of C_d, the closer that 'S' approaches zero. The number, 346,355 is approximately the value returned right before the function returns an 'Out of range' error so the function is programmed to return this value at that point. Note 'S' cannot mathematically be negative and also, 'S' goes out of range when it is less than 0.00001. 'S' will approach zero when the speed of the gas and particle are very nearly equal.

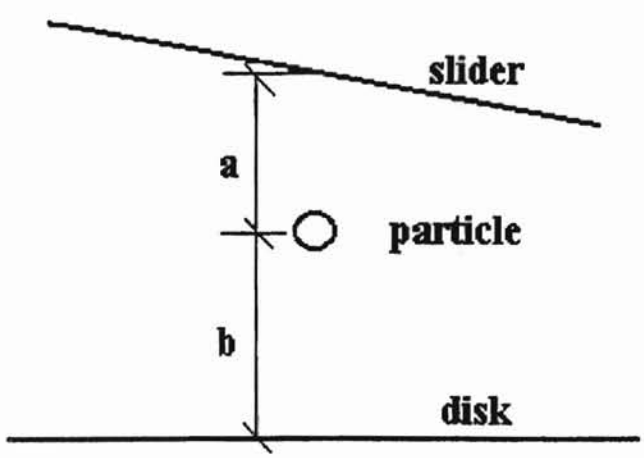

$$
R\_squared\left(X_{in}, Z_{in}\right) := \left|
\begin{array}{l}
a \leftarrow H\left(X_{in}\right) - Z_{in} \\
b \leftarrow Z_{in} \\
r \leftarrow b \\
sign \leftarrow 1 \\
r \leftarrow a \ \text{ if } \ a<b \\
sign \leftarrow -1 \ \text{ if } \ a<b \\
sign \leftarrow 0 \ \text{ if } \ |a-b| \le 0.002 \\
tmp \leftarrow \dfrac{sign}{\left(r \cdot h_m\right)^2} \\
tmp
\end{array}
\right.
$$

$$
R\_squared(1, 0.77) = -2.032098 \cdot 10^{12}
$$

'R_squared( )' is a function that checks which distance is less, a or b (see figure above). Depending on which length is shorter determines to which plate the particle will move. The sign of the function is negative if a is shorter (Qa and Qb carry opposite signs, which coupled with a negative 'a' makes the expression positive and moves the particle in the direction of 'a' (towards the slider).

The Solution

Initial conditions:

$Up_{init} := 1$	Initial 'X-dir' velocity of the particle. Note: $u_p = Up * U_{hat}$
$Wp_{init} := 0$	Initial 'Z-dir' velocity of the particle.
$Xp_{init} := 0$	Initial 'X' position of the particle as it enters the bearing.
$Zp_{init} := 0.5$	Initial 'Z' position of the particle as it enters the bearing..

Note: for this study the 'Y' position is taken at the middle of the recessed region and is taken as constant. Also of note is the assumption that at the instant the particle enters the bearing, its acceleration is assumed zero, i.e. the forces present in the bearing have not had time to effect the particle at T = 0. Likewise, forces from the slider have not had time to act on the gas, so accelerations of the gas at T = 0 is zero. At the boundaries, the pressures are still atmospheric and have zero gradient.

Constants

$Vp_{init} := 0$	Y-direction velocity of the particle is taken as a constant zero, see above.
$Vg := 0$	Gas velocity in 'Y-dir' equals zero, everywhere at middle of wide slider, at any time, t.
$Wg := 0$	Gas velocity in Z equals zero, everywhere, at any time, t.

$$Drag_{prefix} := \frac{3}{4} \cdot R_h \cdot \frac{\rho_g}{\rho_p} \cdot \frac{1}{D_p} \qquad Drag_{prefix} = 289.8119222937$$

$$Saff_{prefix} := \frac{9.69}{\pi} \cdot \frac{R_h}{\sqrt{Re_h}} \cdot \frac{\rho_g}{\rho_p} \cdot \frac{1}{D_p} \cdot \sqrt{\frac{h_m}{U_{hat}}} \qquad Saff_{prefix} = 0.2279725671$$

$$F_{grav} := R_h \cdot \left(\frac{\rho_g}{\rho_p} - 1 \right) \cdot \frac{h_m}{U_{hat}^2} \cdot g_z \qquad F_{grav} = -0.0077023868$$

Electrostatics

$$ParticleVolume := \frac{4}{3} \cdot \pi \cdot \left(\frac{d}{2} \right)^3 \qquad ParticleVolume = 8.1812308687 \cdot 10^{-21} \quad m^3$$

$$BohrRadius := 5.29167 \cdot 10^{-11} m$$

$$HydrogenAtomVolume := \frac{4}{3} \cdot \pi \cdot (BohrRadius)^3 \qquad HydrogenAtomVolume = 6.2067873703 \cdot 10^{-31} \quad m^3$$

$$NumOfHydAtoms := \frac{ParticleVolume}{HydrogenAtomVolume \cdot (9 \cdot 10^9)} \qquad NumOfHydAtoms = 1.4645670906$$

$$CoulombsPerHydAtom := 1.602192 \cdot 10^{-19} coulombs \qquad \frac{HydrogenAtomVolume}{ParticleVolume} = 7.5866180406 \cdot 10^{-11}$$

$$ParticleCharge := NumOfHydAtoms \cdot CoulombsPerHydAtom$$

$$ParticleCharge = 2.346517676 \cdot 10^{-19} \quad coulombs$$

The variable, 'ParticleCharge', sets an upper limit on the charge a spherical debris particle can accumulate. The charge of the disk and slider are assumed to be of like charge in coulombs. The polarity of the charges is arbitrary, as long as the disk and slider have the same polarity. If the particle polarity is the same as the disk/slider, whichever it is closest to will repel it. However, if the polarity of the particle and disk/slider are opposite, then whichever it is closest to will attract it, effectively capturing the particle. For this study, the particle and disk/slider are assumed to be of opposite polarity, therefore whichever the particle is closest to will attract it, i.e., if the particle is closer to the disk, the sign is negative and particle is attracted to the disk. Likewise, if the particle is closest to the slider, the sign is positive and the particle moves toward the slider.

Note: for this study, the particle is assumed to be 'ideally sticky'. Whenever it hits either the slider or the disk, the simulation terminates.

$$Q_a := -ParticleCharge \qquad Q_a = -2.346517676 \cdot 10^{-19}$$

$$Q_b := ParticleCharge \qquad Q_b = 2.346517676 \cdot 10^{-19}$$

Equal, but opposite charges.

$$ElecPrefix := \frac{1.717308 \cdot 10^{10}}{\rho_p \cdot h_m^3 \cdot D_p^3} \cdot \frac{Q_a \cdot Q_b}{\Omega_{hat} \cdot U_{hat}} \qquad ElecPrefix = -1.1882442385 \cdot 10^{-14}$$

'ElecPrefix' contains the equation except $1/r^2$.

Time

$DiskSpeedTime := \frac{L_o}{U_{hat}}$ $DiskSpeedTime = 0.000127$ Time for a point on the disk to travel from front of slider to exit.

$NUMofTimeSteps := 800$

$TimeIncrement := \frac{DiskSpeedTime}{NUMofTimeSteps}$ $TimeIncrement = 1.5875 \cdot 10^{-7}$

$\Delta T := TimeIncrement \cdot \Omega_{hat}$ $\Delta T = 0.0000101063$ Non-dimensional time increment.

$npoints := 10$

'LoopLimit' and 'npoints' are control variables within the solution loop.

$LoopLimit := 6000$

$$D(T,IC) := \begin{bmatrix} 0 \\ 0 \\ 0 \\ 0 \\ IC_0 \cdot \sqrt{(IC_2 - IC_4)^2 + (IC_5)^2} \cdot (IC_2 - IC_4) \\ F_{grav} - IC_0 \cdot (IC_5) \cdot \sqrt{(IC_2 - IC_4)^2 + (IC_5)^2} + IC_1 \cdot (IC_4 - IC_2) + ElecPrefix \cdot IC_3 \end{bmatrix}$$

$$Position := \left| \begin{array}{l} Xp \leftarrow Xp_{init} \\ Zp \leftarrow Zp_{init} \\ Up \leftarrow Up_{init} \\ Wp \leftarrow Wp_{init} \\ tmp2_{0,0} \leftarrow 0 \\ tmp2_{0,1} \leftarrow 0 \\ tmp2_{0,2} \leftarrow Xp \\ tmp2_{0,3} \leftarrow Zp \\ tmp2_{0,4} \leftarrow U_g(Xp, Zp) \\ tmp2_{0,5} \leftarrow Up \\ tmp2_{0,6} \leftarrow Wp \\ \Delta T \qquad\quad 0 \end{array} \right.$$

$$\Delta T_{running} \leftarrow 0$$

$$cnt \leftarrow 0$$

$$Hlimit \leftarrow H(Xp)$$

$$\text{while } (cnt<LoopLimit)\cdot(Xp\le 1)\cdot(Zp\le Hlimit)\cdot(Zp\ge 0)$$

$$\quad Ug \leftarrow U_g(Xp,Zp)$$

$$\quad DragPrefix \leftarrow Drag_{prefix}\cdot C_d(Ug,Up,Wp)$$

$$\quad SaffPrefix \leftarrow Saff_{prefix}\cdot\sqrt{k(Xp,Zp)}$$

$$\quad IC \leftarrow \begin{bmatrix} DragPrefix \\ SaffPrefix \\ Ug \\ R\_squared(Xp,Zp) \\ Up \\ Wp \end{bmatrix}$$

$$\quad tmp1 \leftarrow rkfixed\left(IC,\Delta T_{running},\Delta T_{running}+\Delta T,npoints,D\right)$$

$$\quad Up \leftarrow tmp1_{npoints,5}$$

$$\quad Wp \leftarrow tmp1_{npoints,6}$$

$$\quad newXp \leftarrow Xp+\Delta T\cdot R_L\cdot Up$$

$$\quad newZp \leftarrow Zp+\Delta T\cdot R_h\cdot Wp$$

$$\quad Xp \leftarrow newXp$$

$$\quad Zp \leftarrow newZp$$

$$\quad tmp2_{cnt+1,0} \leftarrow \frac{tmp1_{npoints,0}}{\Omega_{hat}}$$

$$\quad tmp2_{cnt+1,1} \leftarrow \frac{\Delta T_{running}+\Delta T}{\Omega_{hat}}$$

$$\quad tmp2_{cnt+1,2} \leftarrow Xp$$

$$\quad tmp2_{cnt+1,3} \leftarrow Zp$$

$$\quad tmp2_{cnt+1,4} \leftarrow tmp1_{npoints,3}$$

$$\quad tmp2_{cnt+1,5} \leftarrow Up$$

$$\quad tmp2_{cnt+1,6} \leftarrow Wp$$

$$\quad Hlimit \leftarrow H(Xp)$$

$$\quad \Delta T_{running} \leftarrow \Delta T_{running}+\Delta T$$

$$\quad cnt \leftarrow cnt+1$$

$$tmp2$$

$NUMofTsteps := rows(Position) - 1$

$NUMofTsteps = 4549$

$$X_{slider} := \left| \begin{array}{l} \text{for } i \in 0..50 \\ \quad tmp_i \leftarrow \frac{i}{50} \\ tmp \end{array} \right.$$

$$Slider := \overrightarrow{\left[m \cdot \left(X_{slider}^{\langle 0 \rangle} \cdot L_o + b \right) \right]} \cdot \frac{1}{h_m}$$

'X_{slider}' and 'Slider' set up the points to graph the slider on the plot below, while 'X_p' and 'Z_p' pull the correct values to plot from the solution matrix, 'Position'. 'Z_p' is limited to not plot a value above the slider, if it occurs.

$X_p := Position^{\langle 2 \rangle}$

$$Z_p := \left| \begin{array}{l} tmp \leftarrow Position^{\langle 3 \rangle} \\ tmp_{NUMofTsteps} \leftarrow H\left(X_{p_{NUMofTsteps}}\right) \text{ if } Position_{NUMofTsteps,3} > H\left(X_{p_{NUMofTsteps}}\right) \\ tmp_{NUMofTsteps} \leftarrow 0 \text{ if } Position_{NUMofTsteps,3} < 0 \\ tmp \end{array} \right.$$

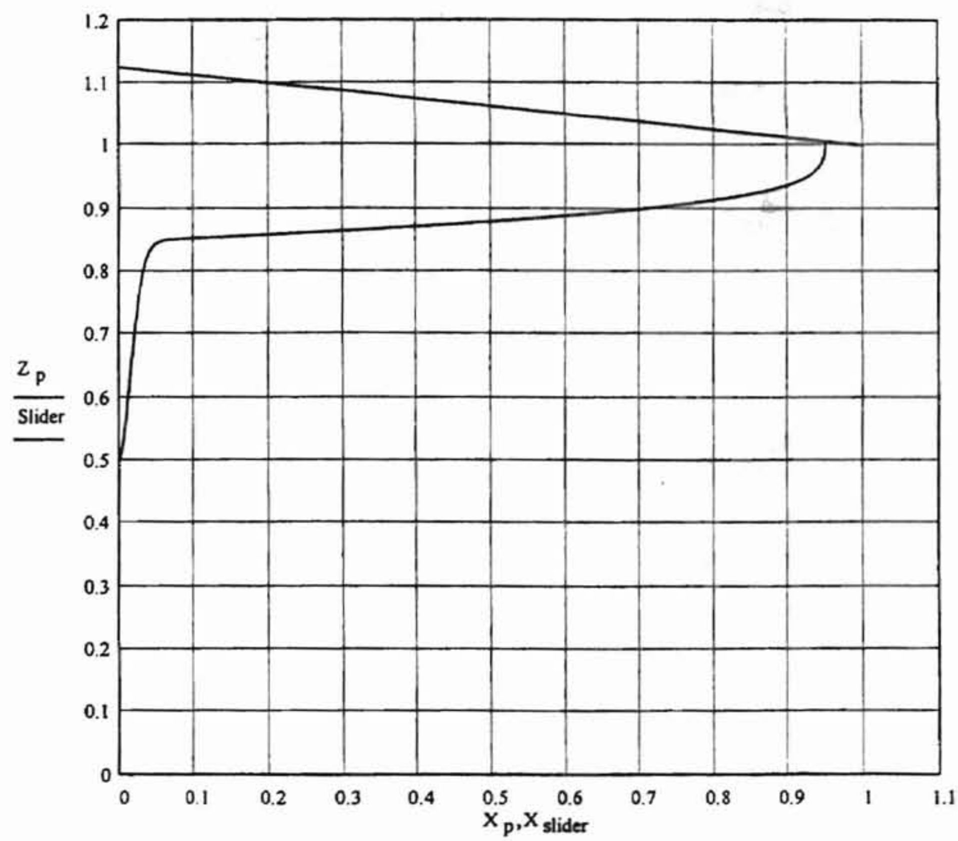

$\text{rows}(X_p) = 4550 \quad \text{rows(Position)} = 4550 \quad vj := \text{cspline}(X_p, Z_p)$

$d = 2.5 \cdot 10^{-7}$

$\text{rows}(Z_p) = 4550 \quad Z_{tmp}(X_{in}) := \text{interp}(vj, X_p, Z_p, X_{in})$

$$
Z_{part} := \left| \begin{array}{l} \text{for } i \in 0..50 \\ \quad \left| \begin{array}{l} tmp_i \leftarrow Z_{tmp}(X_{slider_i}) \text{ if } (X_{slider_i} \le Position_{NUMofTsteps,2}) \\ tmp_i \leftarrow 0 \text{ if } (Z_{p_{NUMofTsteps}} = 0) \cdot (X_{slider_i} > Position_{NUMofTsteps,2}) \\ tmp_i \leftarrow H(X_{slider_i}) \text{ if } (Z_{p_{NUMofTsteps}} = H(X_{p_{NUMofTsteps}})) \cdot (X_{slider_i} > Position_{NUMofTsteps,} \end{array} \right. \\ tmp \end{array} \right.
$$

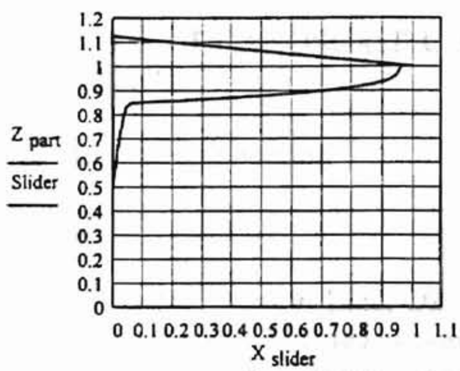

This is a routine to prepare the output to write t an Excel file for plotting purposes. This graph should be identical to the above.

D:\Xslider.xls

X_{slider}

D:\Slider.xls

Slider

D:\Zpart.xls

Z_{part}

VITA

Richmond Harlan Polwort

Candidate for the Degree of

Master of Science

Thesis: MOTION OF NANOSCALE CONTAMINANT PARTICLES IN AIR BEARINGS

Major Field: Civil Engineering

Biographical:

Personal Data: Born in Enid, Oklahoma, on July 31, 1954, the son of Melvin and Vita Polwort. Married to Susan Elaine Polwort (*nee* McMullen) on November 30, 1978. Two children, Brent Andrew Polwort, son, born February 19, 1981, and Liesel Marie Polwort, daughter, born October 19, 1982.

Education: Graduated from Enid High School, Enid, Oklahoma in May 1972; received Bachelor of Science Degree in Civil Engineering from Oklahoma State University, Stillwater, Oklahoma in July 1996; completed the requirements for the Master of Science Degree with a major in Civil Engineering at Oklahoma State University in July, 1999.

Experience: Employed by Farmland Industries, Inc., as a weighmaster/ equipment operator, Enid, Oklahoma, 1977 to 1992. Employed by Oklahoma State University as an undergraduate teaching assistant, Department of Civil and Environmental Engineering, Oklahoma State University, 1996 to 1997. Employed by Envirotech Services, Inc., as a project engineer, Enid, Oklahoma, May 1997 to December, 1998. Employed by The Charles Machine Works, Inc., as plant engineer, Perry, Oklahoma, January 1999 to present.

Professional Memberships: American Society of Civil Engineers, National Society of Professional Engineers, Oklahoma Society of Professional Engineers, Chi Epsilon, Tau Beta Pi, and Phi Kappa Phi honor societies.